OPTIMIZATION AND KINETIC STUDIES ON CORROSION CONTROL OF MILD STEEL USING *IPOMOEA BATATAS* LEAF EXTRACT AS INHIBITOR IN ACIDIC MEDIUM

AJANI, DAVID OPEYEMI

(12BB001812/19000075)

SUBMITTED TO

THE DEPARTMENT OF CHEMICAL ENGINEERING, COLLEGE OF ENGINEERING, LANDMARK UNIVERSITY, OMU-ARAN, KWARA STATE

IN PARTIAL FULFILMENT OF REQUIREMENTS FOR THE AWARD OF MASTERS DEGREE OF ENGINEERING

OCTOBER, 2021.

DECLARATION

I, AJANI, DAVID OPEYEMI, an M.Eng student in the Department of Chemical Engineering, Landmark University, Omu-Aran, hereby declare that this thesis entitled "Optimization And Kinetic Studies On Corrosion Control Of Mild Steel Using *Ipomoea Batatas* Leaf Extract As Inhibitor In Acidic Medium", submitted by me is based on my original work. Any material(s) obtained from other sources or work done by any other persons or institutions have been duly acknowledged.

AJANI, DAVID OPEYEMI (12BB001812)

Signature & Date

CERTIFICATION

This is to certify that this thesis has been read and approved as meeting the requirements of the Department of Chemical Engineering, Landmark University, Omu-Aran, Nigeria, for the Award of M. Eng.

Dr. O. Oyewole	**Date**
(Supervisor)	
Prof. O. S. Bello	**Date**
(Co-Supervisor)	
Dr. B. S. Fakinle	**Date**
(Head of Department)	
Prof. Omodele A. A. Eletta	**Date**
(External Examiner)	

ABSTRACT

Corrosion inhibitors routinely employed in industries are primarily toxic, posing a risk to persons and the environment; thus, green inhibitors made from plant extracts are required. The aim of the study is to investigate the optimization and kinetic studies of mild steel corrosion utilizing *Ipomoea batatas* Leaves extract (IBLE) as an inhibitor in phosphoric acid (H_3PO_4). The extract was subjected to a phytochemical screening to establish the presence of bioactive components. To optimize and study the interactions of the process factors, Box Behnken design was used. Temperature (30 - 60 ^oC), immersion period (5 - 10 days), inhibitor concentration (0.3 - 0.9 g/L), and acid concentration (0.5 - 1.5 M) are the variables employed in the experimental design. The corrosion inhibitory roles of various concentrations of the extracts were investigated using weight loss, electrochemical impedance spectroscopy, and potentiodynamic polarization techniques. Scanning Electron Microscope (SEM), Fourier Transform Infrared Spectroscopy (FTIR), and Energy Dispersive X-ray Florescence (EDXRF) were used to characterize the samples. The presence of saponins, tannins, phenols, steroids, and glycosides in IBLE was confirmed by phytochemical analysis, which suggested the extract as a good inhibitor. The Temperature (45 ^oC), immersion time (5 days), inhibitor concentration (0.9 g/L), and acid concentration (1.0 M) from the experimental design, produced the highest inhibition efficiency of 99.60 %. The variables predicted for the validated optimal process level was (38 ^oC), immersion time (5 days), inhibitor concentration (0.9 g/L), and acid concentration (1.0 M) which yielded an inhibition efficiency of 99.8 %. Electrochemical impedance spectroscopy and potentiodynamic polarization inhibition efficiency were 95.47 % and 83.68 %, respectively. The SEM, FTIR, and EDXRF data revealed that the verified optimal procedure level produced more protective film on the coupon. The enthalpy (ΔH_{ads}) was an endothermic reaction that occurred spontaneously. It was concluded that the *Ipomoea batatas* leaves extract served as a barrier, preventing the acid solution from corroding the mild steel.

Keywords: Corrosion rate, inhibition efficiency, optimization and kinetics.

DEDICATION

This project is dedicated to the Almighty God, as well as my parents, DCP and Mrs Ajani, for their unwavering love and support throughout my study.

ACKNOWLEDGEMENTS

Firstly, I am grateful to the ALL-POWERFUL GOD for His guidance and protection over me throughout the period of my study. With HIM everything has been made possible. All glory is to His name.

I am indeed very grateful to my able and indefatigable supervisor, Dr. O. Oyewole, for her guidance throughout the duration of this research. Her erudite criticisms, encouragement and untiring support made this research work a success. My gratitude also goes to Prof. O. S. Bello, my co-supervisor, for his support and advice on the project. His generosity and support deserve to be emulated. I am extremely thrilled to have both of them as my supervisors.

My profound gratitude also goes to the Chemical Engineering Head of Department, Landmark University, Dr. B. S. Fakinle, as well as the Post-graduate coordinator Dr. A. E. Taiwo for their support and criticism.

I sincerely acknowledge the contributions of Prof. M. Oki, Dr. O. S. Adesina, Engr. J. B. Adeoye, Dr. O. A. Dada, Engr. B. Akinyemi and Engr. K. S. Obayomi towards the improvement of this work. Their advices and discussion made on the subject matter will never be forgotten. I am particularly grateful to the technologists of the Department especially Mr T. S. Abayomi and Mr O. D. Kola for their tireless assistance towards the use of the laboratory and equipment for the research.

My parents' love, kindness, compassion, dedication, and encouragement for me are immeasurable. I owe my siblings, Ajani Ebenezer, Ajani Samuel, and Ajani Emmanuel, an unlimited debt of appreciation for their support and encouragement.

Finally, I would like to thank my friends as well; Otu Steven, Tijani Bashiru, Fadeyi Blessing, Ayoola Ayooluwa, Suleiman Omowumi, Okonta Winifred, Nsikak Nsibiet, Dottie Eworitshe, Chinenye, Ejigboye Praise and Aniobi Mathias for sharing with me their experiences and love during the course of this program.

TABLE OF CONTENTS

LIST OF TABLES

LIST OF FIGURES

LIST OF PLATES

CHAPTER ONE

INTRODUCTION

1.1 Background of Study

Corrosion is the deterioration of metals caused by electro-chemical reactions in the environment (Gutti *et al.,* 2013). It is a fundamental process that affects the global economy and human health. Mild steel is an affordable engineering material by virtue of its properties such as strength, ductility, toughness, malleability, machinability and weld ability (Muthamma *et al.,* 2020). It finds application in automobile components, structural shapes, sheets, petrochemical and oil and gas industries. Corrosion inhibitors are required in acidic media such as those used in industrial acid washing, acid descaling, and acid pickling to prevent metallic components from corroding (Verma *et al.,* 2018).

Corrosion of metals has been a major challenge in industries, which had resulted into high cost in mitigating corrosion. According to National Association of Corrosion Engineers, the annual global cost of corrosion was $2.5 trillion, or approximately 3.4 percent of global GDP (Verma *et al.,* 2017). Implementing corrosion prevention best practices could result in global savings of 15 - 35 % of that cost, or $375 - $875 billion (Hou *et al.,* 2017; Verma *et al.,* 2017; Fu *et al.,* 2021). For more than three decades, corrosion has been a problem in Nigeria's oil and gas industry. Reports showed that some oil companies had their pipeline ruptured due to corrosion, resulting in oil spills which created environmental losses and devastation (Obike *et al.,* 2020). Resources are lost in cleaning up this environmental challenge, which results in large-scale ecological harm due to corrosion effects. As a result, preventing this undesirable phenomenon may be a feasible answer to investigate this problem.

Corrosion inhibition has been described as the most cost-effective method of corrosion mitigation. Corrosion inhibitor is any substance(s) that can effectively reduce the rate of corrosion of the exposed metal, when applied to a corrosive environment (Obike *et al.,* 2020). Inhibitors are divided into two major types which are organic and inorganic inhibitors. Inorganic corrosion inhibitors are effective, but they are largely dangerous to people and the environment. Plant and bio waste extracts (green organic inhibitors) are abundant, inexpensive, nontoxic and biodegradable, so the study of corrosion

control, especially on mild steel, using plant-based and bio waste materials as corrosion inhibitors is of great interest (Umoren *et al.,* 2019). Researchers have made efforts to find appropriate green corrosion inhibitors from natural sources. Some of the extracts that have been used are reported ~~as~~ are: *Rhizophora apiculate* (Rahim *et al.,* 2011), *Citrus aurantifolia* (Haldhar *et al.,* 2019), *Uncaria gambir* (Haldhar *et al.,* 2019), *Neolamarckia cadamba* (Raja *et al.,* 2013), *Glycyrrhia glabra* (Alibakhshi *et al.,* 2018), tea leaves (Hamdan and Haider, 2018), Shrimp waste protein (Farag *et al.,* 2018), coconut coir dusts extract (Umoren *et al.,* 2012), rice straw extract (Mahros *et al.,* 2016), human hair (Verma *et al.,* 2016), Enzyme- and acid-extracted sugar beet pectin (Abou-Elseoud *et al.,* 2021), *Musa acuminate* (Kumar and Yadav, 2020), *Pomelo* peel (Lin *et al.,* 2021), *Arbutus unedo* leaf (Abdelaziz *et al.,* 2021), *Tunbergia fragrans* (Muthukumarasamy *et al.,* 2020), *Monringa oliefera* (Akaleze *et al.,* 2020), *Magnolia kobus* (Chung *et al.,* 2020), *Ammi visnaga* (Aourabi *et al.,* 2021), *Apostichopus japonicas* (Zhang *et al.,* 2021). The activity of chemicals identified in plant and bio waste extracts has been linked to electronegative functional groups and the existence of electrons in triple or conjugated double bonds (Singh *et al.,* 2012c). The research focused on the physical and chemical interactions between the compounds and metal surfaces (Alvarez *et al.,* 2018).

1.2. Problem Statement

Corrosion is a threat to both the environment and industrial activities, making it a major concern in industries. In Nigeria, this has had a negative influence on both major and small industries. Because it is impossible to completely eliminate corrosion, the only viable option is to limit it to the barest minimum. The most prevalent material used in the petrochemical and manufacturing industries is mild steel. The mild steel option as a material of choice offers cost and accessibility advantages. However, because they are constantly interacting with the acid, they are prone to damaging effects over time. The damaging effects become obvious when the load capacity of such facilities like shell thickness become compromised by reduction in the effective diameter as a result of metal loss from corrosive attack. Since the effective diameter cannot support the compressive load, failure is inevitable and often catastrophic.

Methods for preventing corrosion include; material selection, coatings, cathodic/anodic safety, and the use of corrosion inhibitors. Inhibitors have become increasingly popular over the years. Inhibitors are divided into two categories. These

are organic and inorganic/chemical inhibitors. After use, some inorganic inhibitors contaminate the ecosystem and cause plenty of complications, including the loss of plant and animal life. The synthetic organic inhibitors and the green organic inhibitors are sub-divisions of organic inhibitors. Synthetic organic inhibitors have also been used, but their usefulness has been limited due to their toxicity and high production costs (Chigondo & Chigondo, 2016). As a result, researchers have been motivated to look into other areas to substitute inorganic and synthetic organic inhibitors with affordable, environmentally safe, and biodegradable corrosion inhibitors, from agricultural and biological wastes such as plants and animals (green organic inhibitors).

1.3. Justification

Corrosion has a negative effect on health, safety, and the environment, in addition to the financial costs. Corrosion affects every industry, including the oil and gas and resource sectors, as well as nearly every aspect of human life. Therefore, the development of executing successful corrosion mitigation methods is important.

This research will show best interaction of the variables for the control of mild steel corrosion. Also by identifying the active compounds contained in the *Ipomoea batatas* leaf extract. The application of *Ipomoea batatas* leaf extract, (an agricultural by-product and environmentally friendly corrosion inhibitor) is the focus of this research. This bio-waste was utilized to keep mild steel from corroding in Phosphoric acid under various working conditions.

1.4. Aim and objectives of the Research

The aim is to optimize and carry out a kinetic study on corrosion control of mild steel using *Ipomoea batatas* leaves extract (IBLE) as green inhibitor in acidic medium.
The objectives are to:

i. determine the phytochemical constituents of IBLE.
ii. investigate the interactions of the process variables for the corrosion control and determine the optimum conditions.
iii. study the inhibition kinetic parameters governing the corrosion inhibition process.

1.5. Scope of Study

This study was confined to the use of *Ipomoea batatas* leaves extract (IBLE) collected from Offa town, Kwara State, as inhibitor on mild steel in varying concentrations of H_3PO_4. The IBL was extracted using the Soxhlet extractor apparatus. The corrosion inhibition process factors of temperature (30 - 60 ^oC), immersion period (5 - 10 days), inhibitor concentration (0.3 - 0.9 gL^{-1}), and acid concentration (0.5 - 1.5 M) were optimized using Response Surface Methodology (RSM) and Box Behnken design (BBD). The variables considered for the optimization was adopted from Anadebe *et al.*, 2019. Weight loss, Potentiodynamic Polarization, and Electrochemical Impedance Spectroscopy (EIS) techniques were used to determine corrosion inhibition efficiency of IBLE in H_3PO_4. Fourier Transform Infrared Spectroscopy (FTIR), Scanning Electron Microscopy (SEM), and Energy Dispersive X-ray Fluorescence (EDXRF) were used to investigate and characterize the adsorbed extract on the surface of the coupon.

The novel achievement of this research was that *Ipomoea batatas* leaves extract was used in H_3PO_4 via optimization approach; other species of the *Ipomoea batatas* leaves extract could be used in other environment and it can be replicated for use in industries to solve challenges caused by corrosion.

1.6. Significance of Research

Researchers are currently working to create sustainable technology for corrosion mitigation in order to raise ecological awareness and establish environmental standards, limiting the use of toxic inorganic inhibitors.

According to this study, corrosion inhibition and metal/alloy safety are crucial in the chemical, manufacturing, and oil and gas industries. The findings pave the way for researchers to investigate *Ipomoea batatas* leaves extract (IBLE) as a cost-effective and ecologically friendly alternative to corrosion inhibitors such as polyethylene chloride and chromium oxide. The findings will also help combat corrosion in oil service industries by using IBLE as inhibitor due to the fact that it is readily available, biodegradable and environmentally friendly. The use of IBLE as a mild steel corrosion inhibitor is a green technology approach.

CHAPTER TWO

REVIEW OF LITERATURE

2.1. Corrosion

Corrosion comes from the Latin word "corrodere," which means "to tear to pieces." Corrosion is defined as the progressive “wearing away” of metal. It is the gradual deterioration of a material resulting from the unfavourable relation with the environment, which affects structural characteristics of the material. It is a steady degradation as a result of unfavourable contact with the atmosphere, compromising the structural properties and carrying ability of the material (Fayomi *et al.*, 2020). The effects of corrosion are numerous and vary pending on the depth and form of corrosion. Corrosion occurs when the surface layer of a metal gets in contact with a fluid, and the reaction is amplified when in contact with mild temperature, acids, or reactive chemicals (Bupesh *et al.*, 2021). Several researchers have focused on the study of steel under various environmental conditions. Steel corrosion requires the presence of both moisture and oxygen. Temperature, moisture, rain, wind velocity, and solar radiation are all common atmospheric factors that can cause steel corrosion (Soufeiani *et al.*, 2020). Corrosion has resulted in significant economic losses as well as safety issues in human society (Rajabipour & Melchers, 2013; Sachan & Singh, 2020; Liu *et al.*, 2018).

2.2. Forms of Corrosion

Corrosion has happened in all civilizations since the dawn of technology, and it is heavily reliant on the use of metals and alloys. With the exception of certain noble metals like gold, all metals are subject to corrosion (Shreir, 2010). Corrosion can change metals in a variety of ways, based on their structure and the environmental conditions they are exposed to. There are different types of corrosion; the various forms, features, and examples of corrosion are summarized in Table 2.1.

Table 2.1: Corrosion forms, characteristics and examples

Forms	Characteristics	Examples	References
Uniform attack	Corrosion occurs in all areas of the metal at the same or equivalent rates.	Oxidation and tarnishing; active acid dissolution; anodic oxidation and passivity; chemical and electrochemical polishing; and, in some cases, airborne and immersed corrosion.	(Hussain *et al.*, 2020)
Pitting corrosion	Small pits penetrate the metal and can lead to perforation as a result of highly concentrated attack at specific sites.	Pitting of passive metals such as stainless steels, aluminum alloys, and other similar materials in the presence of specific ions, such as chloride ions.	(Balan, 2018)
Selective leaching	One of the alloy's components, typically the most involved, is removed selectively.	The most active is usually withdrawn from the alloy selectively. Graphitization, dezincification, and dealuminification.	(Hussain *et al.*, 2020)
Localized corrosion	Certain areas of the metal surfaces corrode at higher rates than others due to heterogeneities in the metal, the environment or in the geometry of the structure as a whole. Attack ranges from slightly localized to pitting	Deposit attack, bimetallic corrosion, intergranular corrosion, and weld decay are all examples of crevice corrosion.	(Shreir, 2010)

Table 2.1: Corrosion forms, characteristics and examples (Contd)

Forms	Characteristics	Examples	References
Crevice Corrosion	A micro-environmental stagnant solution is linked to this.	Gaskets, washing machines, clamps, lap joints, bolts, and rivet leads are all susceptible to corrosion.	(Tanzi *et al.*, 2019)
Erosion Corrosion	The creation (by corrosion) and degradation (by mechanical process) of a metal's protective film or coating on a regular basis.	Impingement damage, cavitation damage, hydrogen cracking, and corrosion fatigue are all examples of corrosion fatigue.	(Shreir, 2010)
Inter-granular Corrosion	Localized attacks on or close grai boundaries, while the majority of grains are unaffected	A chemical separation effect (impurities appear to be enriched a grain limits) or some processes precipitated on grain boundaries, resulting in decreased corrosion resistance areas in the immediate vicinity.	(Vargel, 2020).
Stress Corrosion Cracking	In a corrosive medium, many alloys are subjected to static surface tensile stress.	The combined effects of tensile stress on the surface trigger cracks	(Shreir, 2010)

2.3. Consequences of corrosion

Corrosion has a variety of consequences, and the influence on the productive operation of equipment and structures is frequently far greater than the loss of metal mass. Failures of various kinds and the need for costly replacements might occur even if the amount of metal lost is low. The following are some of the negative consequences of corrosion (Obike *et al.,* 2020):

1. Mechanical properties are lost as steel thickness decreases, resulting in structural collapse. Even a little quantity of metal loss can cause significant weakness because metal is lost in specific places, resulting in a crack-like structure.
2. Delay in the production of industrial equipment.
3. Liquid poisoning in containers and pipelines (e.g. beer goes cloudy when small quantities of heavy metals are released by corrosion).
4. Human hazards or injuries caused by structural collapse (e.g. bridges, cars, aircrafts).
5. Solid corrosion products damage valves, pumps, and other equipment mechanically.
6. Perforation of vessels and valves, allowing materials to escape and potentially causing environmental damage. If a power plant's condenser tube perforates, corrosive sea water will leak into the boilers.
7. Decline in product value due to deterioration in appearance.

2.4. Inhibitors

Corrosion inhibitor is a product that, when applied to an aggressive media slows the corrosion of exposed metal (Nasab *et al.,* 2019). Steel corrosion can be reduced using a variety of methods, including cathodic safety, electrochemical chlorine removal, and corrosion inhibitors (Cai *et al.,* 2013; Singh *et al.,* 2020; Dehghani *et al.,* 2020; Xu *et al.,* 2021). Corrosion inhibitors are one of the most widely used approaches due to their low cost, ease of usage, and dependability. Depending on their chemical composition, conventional corrosion inhibitors may be categorized as inorganic, organic, or mixed inhibitors. Synthetic nitrite molecules have been one of the most successful carbon steel corrosion inhibitors since 1970s (Lui *et al.,* 2012; Xu *et al.,* 2021). Nitrite reacts with Fe^{2+} to produce Fe_2O_3 barrier (Equation 2.1), which slows down dissolution of steel (Lee *et al.,* 2015; Xu *et al.,* 2021). Inorganic inhibitors, on

the other hand, are restricted in their application because of the toxic effects and high dissolution pace when nitrite levels are low (Garcés *et al.*, 2008). Hence, it is crucial to look into some cost-effective and green inhibitors to make sure steel bars exposed to severe environments are dissolution resistant.

$$2Fe^{2+} + 2OH^- + 2NO_2^- \longrightarrow 2NO_2 \uparrow + Fe_2O_3 + H_2O \qquad \textbf{Equation 2.1}$$

Green inhibitors are expected to be non-toxic and environmentally safe. The green inhibitors limit the rate of corrosion damage by blocking the active sites of corroded metal/alloy surfaces. However, via the adsorption of the inhibitor ions/molecules on the corroding metal surface, the corrosion inhibition process occurs to form more stable films (Magrati *et al.*, 2020).

2.5. Adsorption Isotherm and Thermodynamic studies

According to Ashish & Qursishi (2010), adsorption isotherms identify the degree of contact between the molecules of different inhibitors and the metal surface. This research considered four adsorption isotherms which are:

2.5.1. Langmuir isotherm

Isothermic Langmuir adsorption was estimated using Equation 2.2.

$$\frac{C}{\theta} = \frac{1}{K_{ads}} + \mathrm{C} \qquad \textbf{Equation 2.2}$$

Where θ is the surface layer, C is the concentration (M) and K_{ads} (KJ/mol) is the adsorption process equilibrium constant. The graph of $\frac{C}{\theta}$ versus C was plotted to obtain K_{ads} at different temperature and their correlation coefficient (R^2).

K_{ads} is correlated to the standard free energy of adsorption in Equation 2.3. The calculated K_{ads} was used to calculate ΔG_{ads} at different temperature.

$$K_{ads} = \frac{1}{55.5}\exp\left(-\frac{\Delta G_{ads}}{RT}\right) \qquad \textbf{Equation 2.3}$$

Where R is the universal gas constant ($m^3 \cdot Pa \cdot K^{-1} \cdot mol^{-1}$) and T is the temperature in Kelvin. The calculated K_{ads} (KJ/mol) was used to calculate ΔG_{ads} (KJ/mol) at different temperatures.

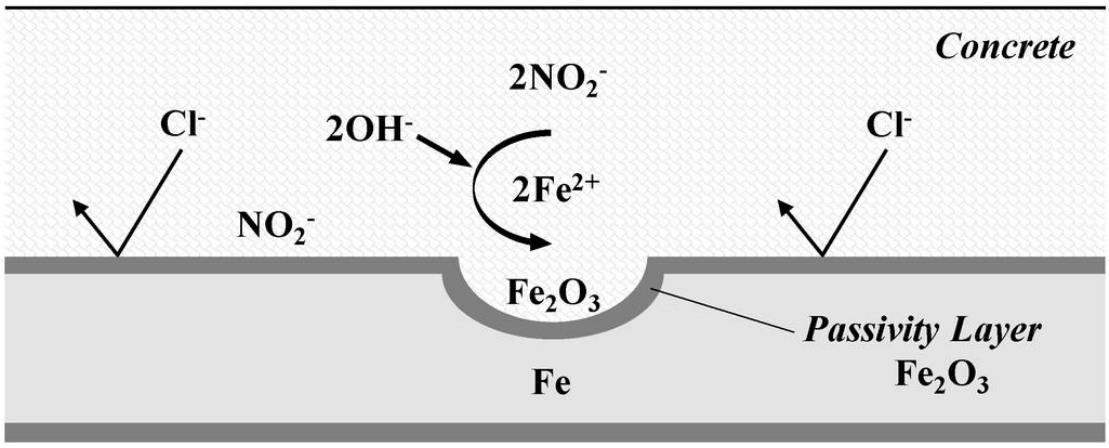

Figure 2.1: Anti-corrosive mechanism of nitrite-based corrosion inhibitors (Source: Lee *et al.,* 2015)

Thermodynamically, ΔG_{ads} (KJ/mol) is related to the enthalpy (ΔH_{ads}) (KJ/mol) and entropy (ΔS_{ads}) (KJ/mol) of the adsorption process in Equation 2.4.

$$\Delta G_{ads} = \Delta H_{ads} - T\Delta S_{ads} \quad \textbf{Equation 2.4}$$

The transition state equation was explained using this equation (Noor and Al moubaraki, 2008)

$$\log \frac{\theta}{1-\theta} = logA + logC - \frac{Q_{ads}}{2.303RT} \quad \textbf{Equation 2.5}$$

Where Q_{ads} (KJ/mol) is the heat of adsorption which is equal to the enthalpy of adsorption (ΔH_{ads}) (KJ/mol) and A is a constant

The Arrhenius equation is expressed using Equation 2.6

$$\ln K = \ln A - \frac{Ea}{RT} \quad \textbf{Equation 2.6}$$

Where K is the equation rate constant; A (L mol^{-1} s^{-1}) is the pre-exponential factor; E_a (KJ/mol) is the activation energy for the reaction of mild steel; R (KJ K^{-1} mol^{-1}) is the value of gas constant; T (K) is the absolute temperature.

2.5.2. Freundlich isotherm

The linear form of Freundlich isotherm is given in Equation 2.7

$$log\,\theta = \log K_{ads} + n \log C \quad \textbf{Equation 2.7}$$

Where C is the concentration (M), θ is the surface layer, n is adsorption indicator and K_{ads} (KJ/mol) is the adsorption process equilibrium constant. A graph of $\log \theta$ against $\log C$ at different temperatures (303, 318, and 333 K), were plotted on a log-log graph and isothermal parameters n and K_{ads} were obtained as slope and intersect of the straight line.

2.5.3. Temkin isotherm

Temkin adsorption isotherm model was estimated using Equation 2.8 (Alinnor, 2012).

$$\theta = \ln C + K_{ads} \quad \textbf{Equation 2.8}$$

Where: C is the concentration (M), θ is the surface layer and K_{ads} (KJ/mol) is the adsorption process equilibrium constant. A graph of θ against $\ln C$ was plotted at various temperatures (303, 318, and 333 K).

2.5.4. Flory-Huggins isotherm

Flory-Huggins adsorption isotherm was estimated using Equation 2.9 (Ebenso *et al.*, 2008)

$$log\frac{\theta}{c} = b\log(1-\theta) + \log K_{ads} \qquad \textbf{Equation 2.9}$$

Where C is the concentration (M) θ is the surface layer, b is the number of adsorbates occupying adsorption sites and K_{ads} (KJ/mol) is the adsorption process equilibrium constant. A graph of log $\frac{\theta}{c}$ against log $(1-\theta)$ was plotted at various temperatures (303, 318 and 333 K).

2.6. Review of past works and research gap

Corrosion of metals/alloys is a major economic threat. Generally, inorganic inhibitors are expensive to produce and the overuse of these inhibitors to control corrosion might have a negative effect in the environment. This necessitates the need for researchers to find an alternative, cost effective approach of controlling corrosion using biological and agricultural wastes as corrosion inhibitors. Table 2.2 summarizes the review of past works using green inhibitors (plant and animal extract). The research gap was obtained from the literature in Table 2.2. It was observed that no study has been conducted on the optimization and kinetic studies using Box Behnken design for controlling corrosion using *Ipomoea batatas* leaf extract as a green corrosion inhibitor in phosphoric acid.

Table 2.2: Review of past works

Inhibitor concentration	Metal	Test Condition	Test Technique	Maximum IE (η %)	References
Eriobotrya japonica (100% v/v)	Mild steel	0.5 M H_2SO_4, 25°C	WL	96.20	Zheng *et al.*, 2018.
Pongamia pinnata (100 ppm)	Mild steel	1 N H_2SO_4, 30°C	WL	94.60	Bhuvaneswari *et al.*, 2018.
Xanthium strumarium (10 mL/L)	Low carbon steel	1 M HCl, 60°C	WL	94.80	Khadom *et al.*, 2018.
Rollinia occidentalis (1.0 g/L)	Carbon steel	1 M HCl, 25°C	Tafel	85.70	Alvarez *et al.*, 2018.
Turbinaria ornata (25 g/L)	Mild steel	1 M HCl, 25°C	EIS	94.50	Krishnan *et al.*, 2018.
Saraca ashoka (100 mg/L)	Mild steel	0.5M H_2SO_4, 25°C	Tafel	95.50	Saxena *et al.*, 2018.
Ginkgo (200 mg/L)	X70 steel	1 M HCl, 45°C	EIS	92.50	Qiang *et al.*, 2018.
Hemerocallis fulva (600 ppm)	Aluminium	1 M H_2SO_4, 303K	WL	89.00	Chung *et al.*, 2020.
BitterKola leaf ($0.9\ g\ L^{-1}$)	Mild steel	1.2 M HCl, 300K	WL	90.00	Valentine *et al.,* 2018.
Polygonatum odaratum (500ppm)	Aluminium	1 M HCl, 303K	WL	94.70	Prabakaran *et al.,* 2018.
Ipomoea batatas peel ($6.67\ g\ L^{-1}$)	Mild steel	0.5 M HCl, 30^oC	WL	93.96	Alhassan *et al.,* 2019.
Ananas comosus (1000 ppm)	Low-carbon steel	1 M HCl 308 K	WL, PP & EIS	97.6	Mobin *et al.,* 2019.
Ziziphora (200 ppm)	Mild steel	1 M HCl	EIS	93	Dehghani, *et al.,* 2020.

Table 2.2: Review of past works (Contd)

Inhibitor concentration	Metal	Test Condition	Test Technique	Maximum IE (η %)	References
Zingiber officinale (100 ppm)	Mild steel	1 M HCl 298.15K–328.15K	PP & EIS	92.5	Gadow *et al.,* 2017.
Tithonia diversifolia (0.1–0.7%)	Mild steel	1 M HCl 30^{o}C	WL, PP & EIS	94.55	Divya *et al.,* 2019.
Cryptocarya nigra (10–1000 mg/L)	Mild steel	1 M HCl	PP & EIS	91	Faiz *et al.,* 2020
Euphorbia heterophylla llinneo (1 g/L)	Mild steel	1.5 M HCl	PP	69	Akinbulumo *et al.,* 2020.
Ficus tikoua (200 mg/L)	Carbon steel	1M HCl	EIS & PP	95.8	Wang *et al.,* 2019.
Cashew waste (80%)	Mild carbon steel	0.1M HCl	WL	80.5	Olawale *et al.,* 2015.
Rice husk (0.25 g/l)	Mild steel	1 M H_2SO_4 30^{o}C	WL	94.24	Olawale *et al.,* 2017.
Chicken nail (0.1 g/l)	Mild steel	2 M H_2SO_4	WL	74.04	Olawale *et al.,* 2019.
Citrus Sinensis	Carbon steel	0.5 M H_2SO_4 & HCl	WL & PP	94.90 & 76.9	Loto *et al.,* 2020.
Luffa cylindrical (1 g/l)	Mild steel	1 M HCl 303–333	WL, PP & EIS	87.98	Ogunleye *et al.,* 2020.
Olea europaea (200–800 mg/l)	Mild steel	1 M NaOH+0.5 M NaCl	EIS	91.9	Ben Harb *et al.,* 2020.

WL: Weight loss

EIS: Electrochemical impedance spectroscopy

PP: Potentiodynamic polarization

CHAPTER THREE

METHODOLOGY

3.1. Preparation of the Extract

The *Ipomoea batatas* leaves obtained from a farm at Offa, Kwara State, were air dried for 6 days, then crushed into powder and sieved to acquire smooth powder. To obtain a homogenous solution, the fine powder was completely soaked in ethanol solution for 24 hours with occasional stirring, and the extract was recovered by filtration. For each extraction, 100 g of the ground leaves was transferred into a beaker (1000 ml) and 1000 ml of analytical grade ethanol was poured into the beaker. The filtrate was subjected to a soxhlet apparatus to separate the ethanol from the extract. The filtrate obtained was used as inhibitor in pure form. The extract was used to make test solutions with concentrations of 0.3 g/L, 0.6 g/L, and 0.9 g/L with 0.5 M, 1.0 M, and 1.5 M of H_3PO_4.

Plate 3.1 shows the *Ipomoea batatas* leaves while Plate 3.2 shows the preparation of *Ipomoea batatas* leaf extract via the Soxhlet apparatus.

3.2. Phytochemical Analysis

The IBL extract was subjected to phytochemical study to ascertain the presence of the active compounds such as: alkaloids, tannins, saponins, flavonoids, glycosides, phenols, and steroids that might be present.

3.2.1 Test for Alkaloids

Component extraction from 2 g of IBLE sample was carried out by boiling 5 % tetraoxosulphate (VI) acid (H_2SO_4) (20 cm^3) in 50 % ethanol for 2 minutes and then filtering through Whatman filter paper (125 mm). Using a separating funnel, 5 cm^3 of 28 % ammonia solution (NH_3) was used to make the filtrate alkaline. Further solution extraction was carried out using an equal amount of chloroform (5.0 cm^3), which was extracted with two 5 cm^3 portions of 1.0 M dilute tetraoxosulphate (VI) acid. The following test was subsequently performed using the final acid extract: 2 cm^3 acid extract was combined with 0.5 cm^3 Dragendorff's reagent (Bismuth potassium iodide solution). This method was adopted from Ezeonu & Ejikeme, 2016.

Plate 3.1: *Ipomoea batatas* leaves

Plate 3.2: Extraction of *Ipomoea batatas* leaves

3.2.2 Test for Tannins

In a water bath containing 30 cm^3 of water, 0.30 g of IBLE was weighed and boiled for 10 minutes. Filtration was carried out after boiling using Whatman filter paper (125 mm). Three drops of 0.1 % ferric chloride were applied to 5 cm^3 of the filtrate. This methodology was adopted from Ejikeme *et al.,* 2014.

3.2.3 Test for Saponins

Water bath with a volume of 30 cm^3 of water, 0.30 g of IBLE was boiled for 10 minutes and filtered using Whatman filter paper (125 mm). A mixture of 5 cm^3 of distilled water with 10 cm^3 of filtrate was centrifuged for a stable persistent froth. This analysis was adopted from Ejikeme *et al.,* 2014.

3.2.4 Test for Flavonoids

IBLE (0.30 g) was weighed and transferred into a beaker. The IBLE was extracted with 30 cm^3 of distilled water at room temperature, for 2 hours and filtered with Whatman filter paper (125 mm). 10 cm^3 of the aqueous filtrate of the IBLE was added to 5 cm^3 of 1.0 M of dilute ammonia solution, thereafter; 5 cm^3 of concentrated tetraoxosulphate (VI) acid was added. This method was adopted from Ezeonu & Ejikeme, 2016.

3.2.5 Test for Glycosides

In a water bath, 2.0 g of IBLE was added to 20 cm^3 of water, boiled for 5 minutes, then filtered using Gem filter paper (12.5 cm). 5 cm^3 of the filtrate was mixed with 0.2 cm^3 of Fehling's solutions A and B until it became alkaline (tested with litmus paper). This procedure was adopted from Ezeonu & Ejikeme, 2016.

3.2.6 Test for Phenols

To get a 20 % concentration, 20 μL of IBLE was mixed with 1.16 mL of distilled water, 100 μL of Folin-Ciocalteu reagent, and 300 μL of sodium carbonate (Na_2CO_3). The mixture was incubated at 40 °C for 30 minutes before being measured at 760 nm with a spectrophotometer. This procedure was adopted from Ammor *et al.,* 2018.

3.2.7 Test for Steroids

IBLE (0.30 g) was weighed and transferred into a beaker. This was combined with 20 cm^3 of ethanol, and after 2 hours, the component was extracted. 5 cm^3 of the ethanolic

extract was added to 2 cm^3 acetic anhydride followed with 2 cm^3 of concentrated tetraoxosulphate (VI) acid. This methodology was adopted from Ejikeme *et al.,* 2014.

3.3. Metal Preparation

Mild steel was obtained from the Mechanical Engineering workshop at Landmark University in Omu-Aran, Kwara State, Nigeria. The mild steel was cut into coupons with dimensions of 20 mm by 25 mm, a thickness of 10 mm, and a 10 mm hole was bored in the centre of the coupon. To expose the shiny surface, each coupon was cleaned with emery paper and washed with distilled water, then degreased in acetone. The coupons were stored in a desiccator for further use. Plate 3.3 shows mild steel coupons.

3.4. Acid Preparation

1 L of 0.5 M, 1.0 M and 1.5 M of H_3PO_4 were obtained from 85 % concentrated H_3PO_4 by diluting 33.9 mL, 67.8 mL and 101.7 mL of the concentrated acid in 1 L of distilled water. The calculation is as shown in appendix VII.

3.5. Experimental Design

Response surface methodology (RSM) is a statistical tool used to analyse the interaction between variables and one or more response. The RSM method involves the design of a series of experiments, adequate response measurements and the creation of a second-order response surface mathematical model with the best fittings. The design expert software was used to analyse the data. The type of design used from the RSM, is the Box Behnken design (BBD). The Box Behnken Design (BBD) generated twenty-nine experimental runs from the design expert software. This experimental runs were conducted based on the interaction of the variables which include; temperature (3 0- 60 ^oC), time of immersion (5 - 10 days), inhibitor concentration (0.3 - 0.9 gL^{-1}) and acid concentration (0.5 - 1.5 M). Experimental ranges of the variables for IBL extract on mild steel in H_3PO_4 solution is shown in Table 3.1. Matrix layout for coded and actual is shown in Table 3.2 and 3.3 respectively.

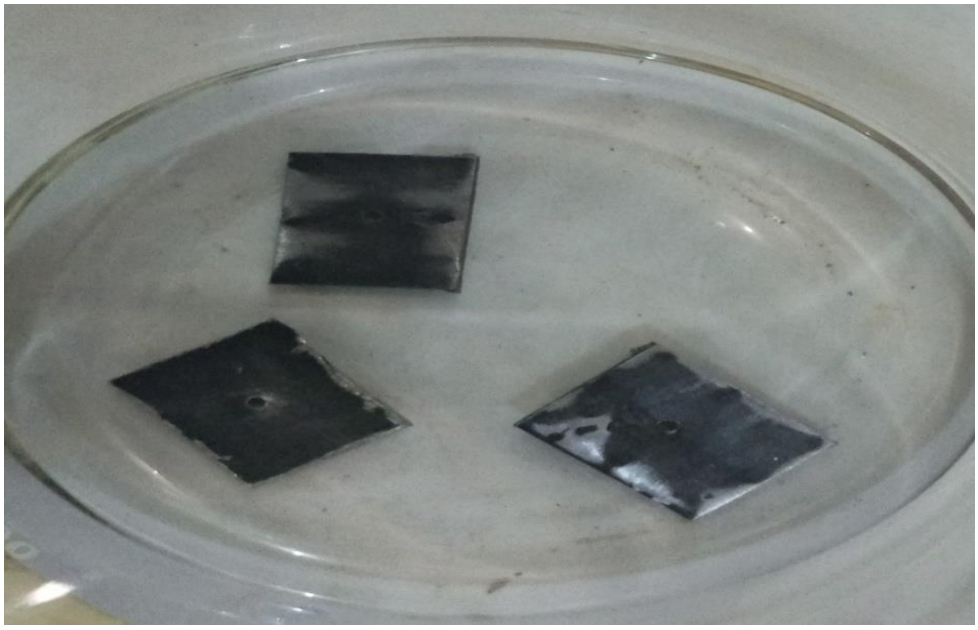

Plate 3.3: Mild steel coupons

3.6. Weight Loss Measurement

Weight loss measurements were performed with time variations of 5 – 10 days as observed from the experimental design. Immersion was conducted using conical flasks containing a formulated solution of acid and inhibitor at specific temperature levels that were retained in a laboratory water bath. Before immersing the coupons into the acid and inhibitor solution, the coupons were weighed. The coupons were collected for each run at particular time of immersion, temperature, inhibitor concentration and acid concentration. After the mild steel coupons had been immersed, they were removed, thoroughly washed to eliminate corrosion impurities, rinsed with distilled water, and finally degreased in acetone. After that, the mild steel was reweighed to determine the weight loss by calculating the difference in weight both before and after immersion. Equations 3.1, 3.2, 3.3, and 3.4 were used to determine the weight loss, corrosion rate, inhibition effectiveness, and surface coverage, respectively. This methodology was adopted by the works done by (Olawale *et al.,* 2017; Anadebe *et al.,* 2019; Emory *et al.,* 2020; Ogunleye *et al.,* 2020.

$W_b - W_a$ **Equation 3.1**

$$CR = \frac{\Delta W}{At}$$ **Equation 3.2**

$$(IE\%) = \frac{CR_{Cont} - CR_{inh}}{CR_{COnt}}(100)$$ **Equation 3.3**

Surface coverage $(\theta) = \frac{IE\ \%}{100}$ **Equation 3.4**

Where W_b is the weight before immersion, W_a is the weight after immersion, ΔW is the weight loss (g) after immersion time, A is the area of the specimen (cm^2) and t is the time of immersion in hours, CR is the corrosion rate at each immersion time, CR_{Cont} is the corrosion rate of metal sample in acid media, CR_{inh} is the corrosion rate of metal sample in the presence of the inhibitor and the acid. *IE %* is the Inhibition efficiency.

Table 3.1: Variables of the low coded and high coded of *Ipomoea batatas* leaves extract on mild steel in H_3PO_4 solution.

Factor	Name	Units	Type	Low Actual	High Actual	Low Coded	High Coded
A	Temperature	°C	Numeric	30	60	-1.000	1.000
B	Time	Days	Numeric	5	10	-1.000	1.000
C	Inhibitor Concentration	gL^{-1}	Numeric	0.3	0.9	-1.000	1.000
D	Acid Concentration	M	Numeric	0.5	1.5	-1.000	1.000

Table 3.2: Matrix of the coded factors

Std	Run	Factor 1 A: Temperature (°C)	Factor 2 B: Immersion Time (days)	Factor 3 C: Inhibitor Conc (gL^{-1})	Factor 4 D: Acid Conc (M)
24	1	0	1	0	-1
5	2	0	0	-1	0
10	3	1	0	0	1
4	4	1	1	0	-1
12	5	1	0	0	0
6	6	0	0	1	0
3	7	-1	1	0	0
28	8	0	0	0	-1
27	9	0	0	0	1
21	10	0	-1	0	-1
8	11	0	0	1	1
22	12	0	1	0	-1
7	13	0	0	-1	1
29	14	0	0	0	0
17	15	-1	0	-1	0
19	16	-1	0	1	0
26	17	0	0	0	0
9	18	-1	0	0	-1
14	19	0	1	-1	0
25	20	0	0	0	0
2	21	1	-1	0	0
15	22	0	-1	1	0
23	23	0	-1	0	1
1	24	-1	-1	0	0
11	25	-1	0	0	1
13	26	0	-1	-1	0
16	27	0	1	1	0
18	28	1	0	-1	0
20	29	1	0	1	0

Table 3.3: Matrix of the actual factors

Std	Run	Factor 1 A: Temperature (°C)	Factor 2 B: Immersion Time (days)	Factor 3 C: Inhibitor Conc (gL^{-1})	Factor 4 D: Acid Conc (M)
24	1	45	10.0	0.6	1.5
5	2	45	7.5	0.3	0.5
10	3	60	7.5	0.6	0.5
4	4	60	10.0	0.6	1.0
12	5	60	7.5	0.6	1.5
6	6	45	7.5	0.9	0.5
3	7	30	10.0	0.6	1.0
28	8	45	7.5	0.6	1.0
27	9	45	7.5	0.6	1.0
21	10	45	5.0	0.6	0.5
8	11	45	7.5	0.9	1.5
22	12	45	10.0	0.6	0.5
7	13	45	7.5	0.3	1.5
29	14	45	7.5	0.6	1.0
17	15	30	7.5	0.3	1.0
19	16	30	7.5	0.9	1.0
26	17	45	7.5	0.6	1.0
9	18	30	7.5	0.6	0.5
14	19	45	10.0	0.3	1.0
25	20	45	7.5	0.6	1.0
2	21	60	5.0	0.6	1.0
15	22	45	5.0	0.9	1.0
23	23	45	5.0	0.6	1.5
1	24	30	5.0	0.6	1.0
11	25	30	7.5	0.6	1.5
13	26	45	5.0	0.3	1.0
16	27	45	10.0	0.9	1.0
18	28	60	7.5	0.3	1.0
20	29	60	7.5	0.9	1.0

3.7. Electrochemical Measurements

3.7.1 Potentiodynamic Polarization

Tafel polarization measurements were performed using a computer-controlled potentiostat/galvanostat (Autolab PGSTAT 302N, Covenant University, Otta, Ogun State) electrochemical device. The platinum electrode was used as the counter electrode (CE), Ag/AgCl as the reference electrode (RE) in 1M H_3PO_4 and the steel sample as the working electrode (WE). For the polarization measurements at 45^{o}C, a traditional three-electrode Pyrex glass cell was used. Test specimens with 1 cm^2 of exposed area were, however, used for each measurement as a working electrode with a lugging probe mounted near the working electrode and all of the experiments were carried out in stagnant aerated solutions.

A stable open circuit potential was achieved by immersing the working electrode in test solution for one hour. The potentiodynamic polarization analysis was carried out using a linear sweep technique at a scan rate of 1 m V/s at a potential range of -250mV + 250 mV with respect to the corrosion potential. When a stable open circuit potential was reached, the working electrode was immersed in a test solution for 1 hour.

The potentiodynamic polarization analysis was performed at a potential range of (E = E_{corr} ± 250 mV) with a scan rate of 0.01 s with respect to the corrosion potential using a linear sweep technique. The corrosion current densities were determined by extrapolating the linear Tafel segments of the anodic and cathodic curves to equilibrium potential (Icorr). The experiments were carried out using the blank and extract concentrations of: 0.3 g/L; 0.6 g/L and 0.9 g/L respectively. This methodology was adapted from the work done by Onukwuli *et al.,* 2020; Annes *et al.,* 2018 respectively. The Tafel inhibition efficiency (IE_T %) was obtained using Equation 3.5.

$$IE_T\ \% = \frac{Icorr_{Cont} - Icorr_{inh}}{Icorr_{Cont}}(100) \qquad \textbf{Equation 3.5}$$

Where: $Icorr_{Cont}$ = uninhibited solution corrosion current density and $Icorr_{inh}$ = inhibited corrosion current densities

3.7.2 Electrochemical Impedance Spectroscopy

Electrochemical test was performed using NOVA 2.0 auto-lab (Covenant University, Otta, Ogun State). The electrochemical impedance study was carried out in 10 $\mathscr{M}$A-10 nA AC signal with a frequency of 0.00001 MHz to 0.01 MHz. This was applied to the device with amplitude of 0.01. The experiments were carried out at 45 ^{o}C using the blank and extract concentrations of: 0.3 g/L; 0.6 g/L and 0.9 g/L respectively. The EIS plot was fitted and used to measure the inhibition efficiency using Equation 3.6, to generate the charge transfer resistance.

$$IE = \frac{R^{i}_{ct} - R_{ct}}{R_{ct}}(100) \qquad \textbf{Equation 3.6}$$

Where: R^{i}_{ct} and R_{ct} are charge transfer resistance in the presence and absence of the inhibitor respectively.

3.8. Kinetic Study

The rate of reaction is given by Equation 3.7 (Khadom & Abdul-Hadi, 2014; Yaro *et al.*, 2013b; Hassan *et al.*, 2016).

$$\frac{dW}{dt} = KW^{n} \qquad \textbf{Equation 3.7}$$

Where k is rate constant and n is the order of reaction. Equation 3.7 can be integrated for different values of reaction order (n). Three reaction models were suggested; Pseudo zero, first and second order models. The integrated forms for zero, first and second orders are given in equation 3.8, 3.9 and 3.10, respectively.

$$K = \frac{W_i - W_t}{t} \qquad \textbf{Equation 3.8}$$

$$W_i = W_t \ \exp(kt) \qquad \textbf{Equation 3.9}$$

$$K = \frac{1}{t}\left(\frac{1}{W_i} - \frac{1}{W_t}\right) \qquad \textbf{Equation 3.10}$$

Where W_t (g) is the mild steel consumption at any time, and W_i (g) is the initial mild steel concentration. Graphs of WL against t, *ln* WL against t and 1/WL against t were plotted for zero, first and second order, respectively for 0.6 gL^{-1} inhibitor concentration and at temperatures of 303, 318 and 333 K.

3.9. Surface Characterization

3.9.1. The Scanning Electron Microscopy (SEM)

SEM (SEM, JCOL-model JSM-6390, Umaru Musa Yar'adua University, Katsina) was used to analyse the surface morphology of the coupon immersed in 1 M H_3PO_4 solution at 45 ^oC (blank), the coupon immersed in 1 M H_3PO_4 solution at 45 ^oC with IBLE (highest inhibition efficiency from the experimental run), and the coupon immersed in 1 M H_3PO_4 solution at 38 ^oC with IBLE (validated experiment).

3.9.2. Fourier Transform Infrared Spectrometer (FT-IR)

FTIR (Infrared spectrometer Varian 660 MidIR Dual MCT/DTGS Bundle, Shmadzu Microlab, ABUAD, Ado-Ekiti) was used to identify the chemical structure and functional groups of the blank solution, the adsorbed corrosion film on the surface of the coupon after immersion in (temperature (45 ^oC); immersion time (5 days); inhibitor concentration (0.9 gL^{-1}); acid concentration (1.0 M) for the highest inhibition efficiency as observed in the experimental run and the adsorbed corrosion film of the validated optimal process levels in temperature (45 ^oC); immersion time (5 days); inhibitor concentration (0.9 gL^{-1}); acid concentration (1.0 M), after immersion.

3.9.3. Energy dispersive X-ray Fluorescence (EDXRF)

EDXRF (EDXRF spectrometer, PW 4052/47B, Umaru Musa Yar'adua University, Katsina) was used to determine the elemental compositions of the coupon immersed in 1 M H_3PO_4 solution at 45 ^oC (blank), the coupon immersed in 1 M H_3PO_4 solution at 45 ^oC with IBLE (highest inhibition efficiency from the experimental run), and the coupon immersed in 1 M H_3PO_4 solution at 38 ^oC with IBLE (validated experiment).

CHAPTER FOUR

RESULTS AND DISCUSSION

4.1. The Result of (IBLE) Phytochemical Analysis

Findings from the phytochemical analysis indicated that IBLE contained bioactive organic compounds (metabolites) that were responsible for the inhibitory properties of a good inhibitor (Table 4.1). This exhibited the existence of saponins, steroids, phenols, tannins, and glycosides. Saponins and phenol were found to be widely available, while steroids, tannins, and glycosides were found to be moderately present. These findings confirmed the result reported by Emembolu *et al.,* 2020, Uwah *et al.,* 2013, and Umoren *et al.,* 2016, Pradeep Kumar & Mohana, 2014, Deng and Xianghong, 2012, Olawale *et al.,* 2019, and Okewale *et al.,* 2020. The result quantitative analysis for the bioactive compounds present in IBLE is shown in appendix VI.

4.2. Result of Weight Loss Measurement

Table 4.2 shows the response(s) for corrosion inhibition on corrosion rate, inhibition effectiveness, and surface coverage responses. Experiment Number (22) as observed from the experimental design: at temperature of 45 ^{o}C, immersion period of 5 days, inhibitor concentration of 0.9 g/L, and acid concentration of 1.0 M revealed that IBLE is an effective mild steel corrosion inhibitor in H_3PO_4, with a 99.6 % inhibition performance and a corrosion rate of 0.0000167 (g/cm^2.hr). The result of the inhibition efficiency confirmed the findings of the study by Noyel *et al.,* (2015); Sivaraju & Kannan (2010); Messali *et al.,* (2017). Although, the inhibition efficiency obtained from this study is higher than what was reported by the researchers mentioned above. This showed that IBLE is a highly effective inhibitor. The inhibition efficiencies of the researchers mentioned above is shown in Table 4.3.

Table 4.1: Result of Phytochemical Component IBLE

Test	Confirmation
Saponins	+++
Steroid	++
Phenol	+++
Tannin	++
Glycoside	++
Flavonoid	--
Alkaloid	--

--: not present ++: moderately present, +++: highly present

Table 4.2: Box Behnken Design layout showing values of weight loss, corrosion rate, inhibition efficiency and surface coverage of mild steel, varying temperature, time, inhibitor concentration and acid concentration

Std	Run	Factor 1 A: Temperature (°C)	Factor 2 B: Immersion Time (days)	Factor 3 C: Inhibitor Conc (gL^{-1})	Factor 4 D: Acid Conc (M)	Response 1 Weight loss (g)	Response 2 Corrosion rate ($g/cm^2.hr$)	Response 3 Inhibition Efficiency (%)	Surface coverage (ɵ)
24	1	45	10.0	0.6	1.5	0.51	0.0004250	92.61	0.9261
5	2	45	7.5	0.3	0.5	0.46	0.0005100	76.28	0.7628
10	3	60	7.5	0.6	0.5	0.07	0.0000778	96.83	0.9683
4	4	60	10.0	0.6	1.0	0.31	0.0002580	93.86	0.9386
12	5	60	7.5	0.6	1.5	0.24	0.0002670	95.36	0.9536
6	6	45	7.5	0.9	0.5	0.02	0.0005670	73.63	0.7363
3	7	30	10.0	0.6	1.0	0.18	0.0001500	96.00	0.9600
28	8	45	7.5	0.6	1.0	0.51	0.0003670	91.26	0.9126
27	9	45	7.5	0.6	1.0	0.51	0.0003670	91.26	0.9126
21	10	45	5.0	0.6	0.5	0.22	0.0003670	85.20	0.8520
8	11	45	7.5	0.9	1.5	0.07	0.0000778	98.65	0.9865
22	12	45	10.0	0.6	0.5	0.14	0.0001170	94.57	0.9457
7	13	45	7.5	0.3	1.5	2.17	0.0024100	58.09	0.5809
29	14	45	7.5	0.6	1.0	0.51	0.0003670	91.26	0.9126
17	15	30	7.5	0.3	1.0	0.17	0.0001890	95.50	0.9550
19	16	30	7.5	0.9	1.0	0.04	0.0000440	98.95	0.9895
26	17	45	7.5	0.6	1.0	0.51	0.0003670	91.26	0.9126
9	18	30	7.5	0.6	0.5	0.22	0.0002440	88.65	0.8865
14	19	45	10.0	0.3	1.0	0.92	0.0007670	81.74	0.8174
25	20	45	7.5	0.6	1.0	0.51	0.0003670	91.26	0.9126
2	21	60	5.0	0.6	1.0	0.24	0.0004000	90.48	0.9048

Table 4.2: Box Behnken Design layout showing values of weight loss, corrosion rate, inhibition efficiency and surface coverage of mild steel, varying temperature, time, inhibitor concentration and acid concentration (Contd)

Std	Run	Factor 1 A: Temperature (°C)	Factor 2 B: Immersion Time (days)	Factor 3 C: Inhibitor Conc (gL^{-1})	Factor 4 D: Acid Conc (M)	Response 1 Weight loss (g)	Response 2 Corrosion rate ($g/cm^2.hr$)	Response 3 Inhibition Efficiency (%)	Surface coverage (ɵ)
15	22	45	5.0	0.9	1.0	0.01	0.0000167	99.60	0.9960
23	23	45	5.0	0.6	1.5	0.37	0.0006170	89.27	0.8927
1	24	30	5.0	0.6	1.0	0.13	0.0002170	94.84	0.9484
11	25	30	7.5	0.6	1.5	0.16	0.0001780	96.90	0.9690
13	26	45	5.0	0.3	1.0	0.59	0.0009830	76.60	0.7660
16	27	45	10.0	0.9	1.0	0.03	0.0000250	99.40	0.9940
18	28	60	7.5	0.3	1.0	1.49	0.0016560	60.56	0.6056
20	29	60	7.5	0.9	1.0	0.08	0.0000898	97.88	0.9788

Table 4.3: Comparison of natural inhibitors for steel in phosphoric acid

Metal	Inhibitor	Concentration of acid	Inhibition efficiency	References
Mild steel	*Psidium guajava*	1 M	89	Noyel *et al.*, (2015)
Mild steel	*Acalypha indica* Leaf	1 N	90.38	Sivaraju and Kannan (2010)
Carbon steel	Guar gum	2 M	95.8	Messali *et al.*, 2017
Mild steel	*Ipomoea batatas* leaf	1 M	99.6	This research

Increase in IBLE concentration improved the inhibition effectiveness, which was more visible due to adsorption of the active compounds. On the corroding mild steel, the IBLE developed a protective film which was observed from Figure 4.9. The anti-corrosion behaviour of the IBLE could be due to the structural characteristics of the heteroatoms that make up the substance (Olasehinde, 2018).

Temperature increase, reduced inhibition efficiency by expelling the IBLE molecules from the mild steel surface thus, separating the IBLE's heterocyclic bonds resulting in less surface coverage (Anadebe *et al.*, 2019). This implied that Immersion period, temperature, acid concentration, and extract concentration all influence mild steel dissolution rate and inhibitory effectiveness in H_3PO_4. Figure 4.1a represent plot of predicted vs. actual for corrosion rate, while Figure 4.1b shows the plot of predicted vs. actual for inhibition efficiency. The comparison of natural corrosion inhibitors for steel in phosphoric acid are shown in Table 4.3.

4.3. 3-D Plots

The impact of the dosage of inhibitors and acid concentration on the rate of corrosion and inhibition effectiveness are shown in Figures 4.2a and 4.3a, respectively. Increase in IBLE concentration resulted in lower degradation rates and higher inhibition effectiveness, culminating in outstanding percentage inhibition (Table 4.2).

The relationship between temperature and acid concentration is negative, as seen in Figures 4.2b and 4.3b. When both variables rose, the corrosion rate increased, reducing the inhibitor's effectiveness. The rate of corrosion increased at higher temperatures.

The relationship between temperature and inhibitor quantity is depicted in Figures 4.2c and 4.3c. As the temperature increased, the amount of IBLE compounds clinging to the surface reduced, resulting in a decrease in surface coverage. Increased inhibitor concentration, on the other hand, improves the physical manifestation of the adsorption film, resulting in significant metal surface coverage.

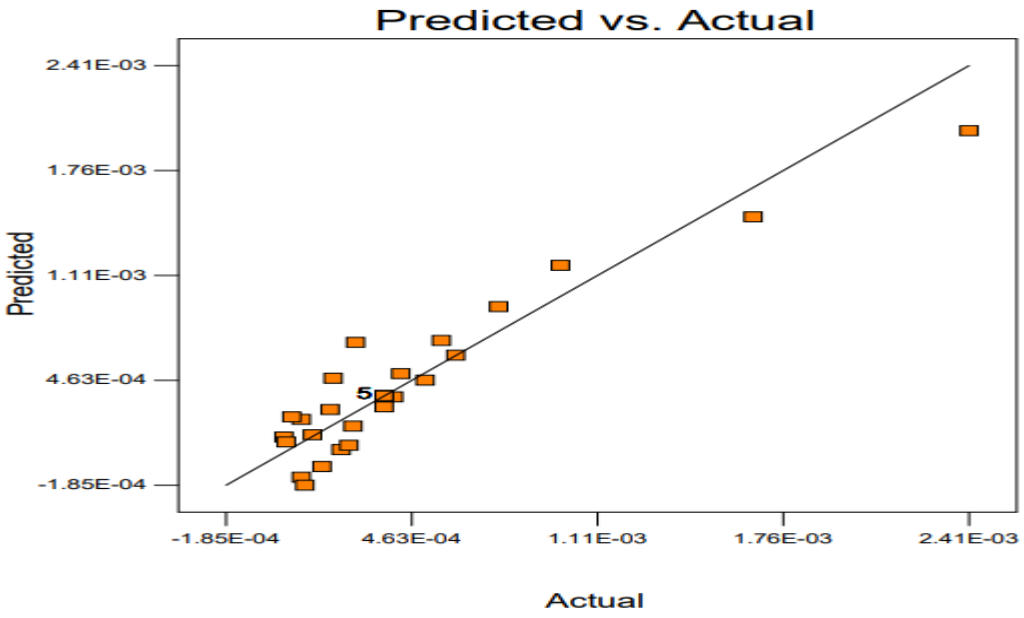

Figure 4.1a: layout of predicted vs. actual for corrosion rate.

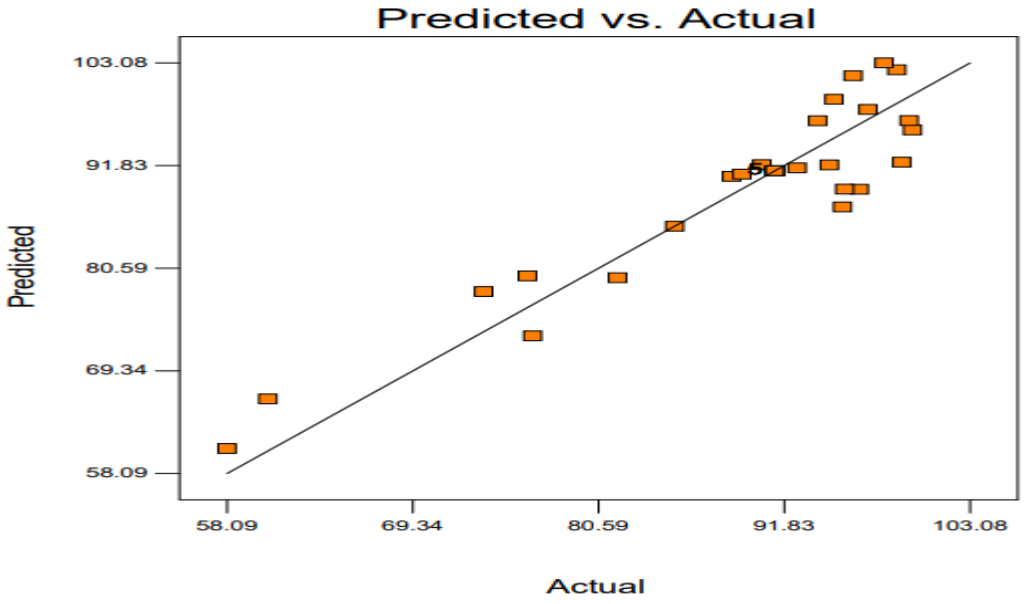

Figure 4.1b: layout of predicted vs. actual for inhibition efficiency.

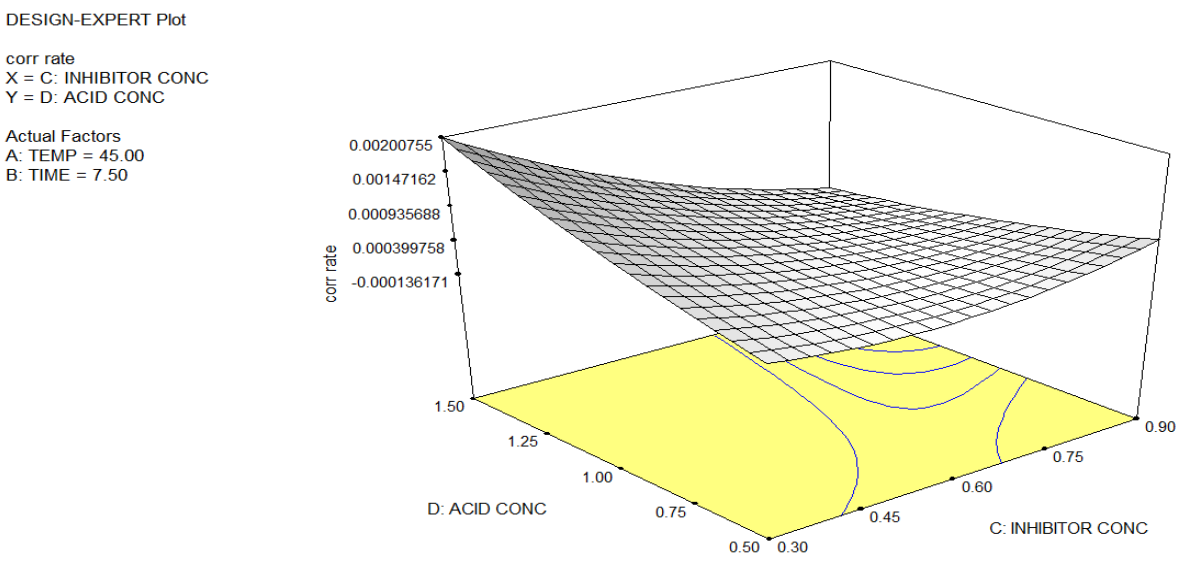

Figure 4.2a: 3-D model plot for corrosion rate of acid concentration versus inhibitor concentration

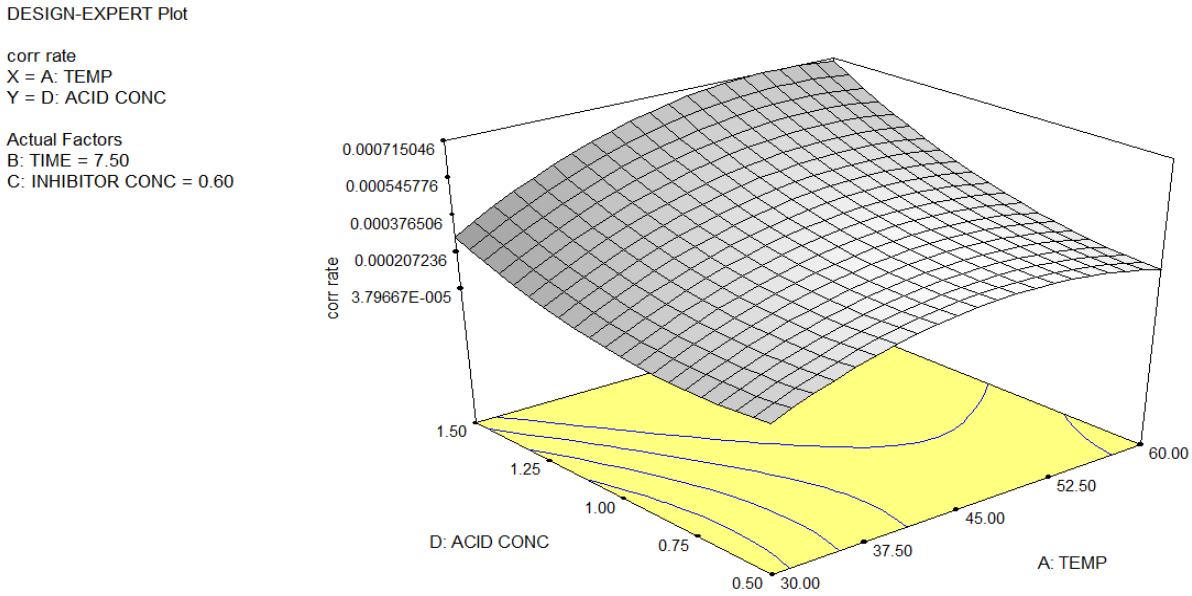

Figure 4.2b: 3-D model plot for corrosion rate of acid concentration versus temperature

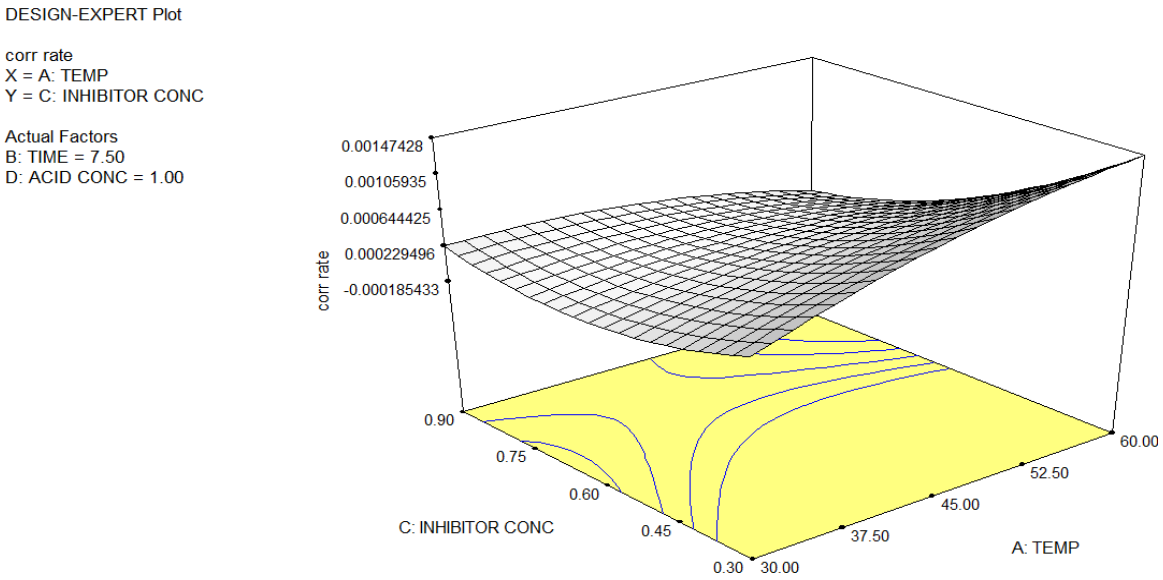

Figure 4.2c: 3-D model plot for corrosion rate of inhibitor concentration versus temperature

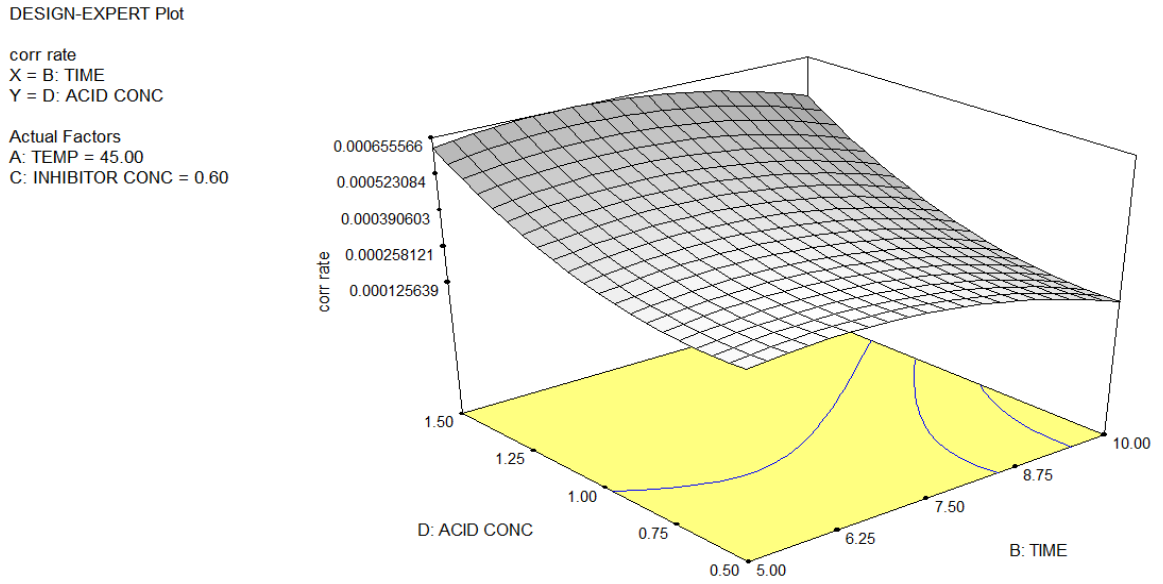

Figure 4.2d: 3-D model plot for corrosion rate of acid concentration versus immersion time

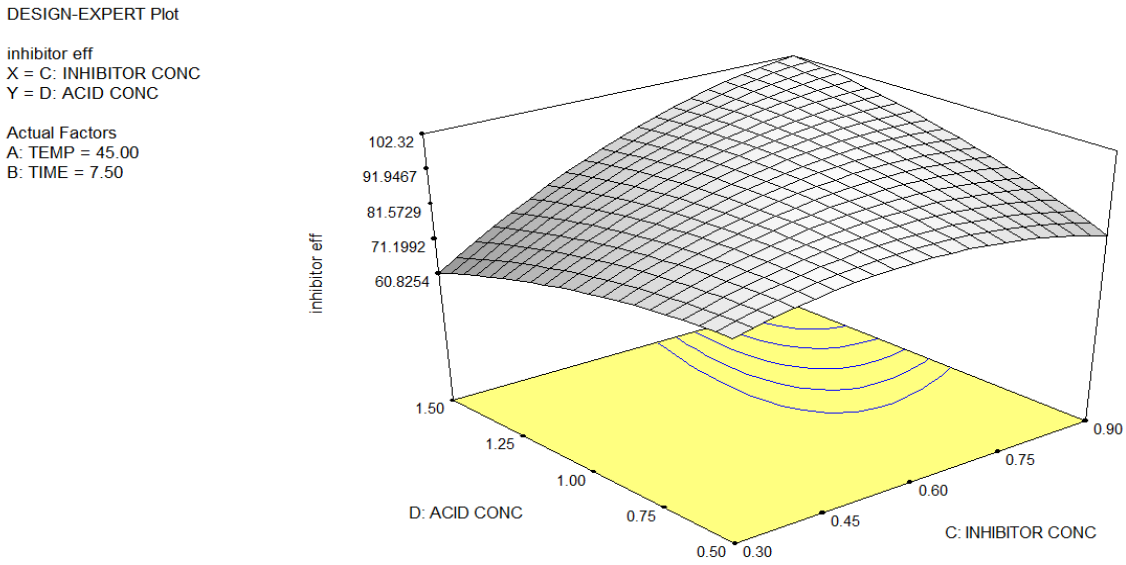

Figure 4.3a: 3-D model plot for inhibition efficiency of acid concentration versus inhibitor concentration

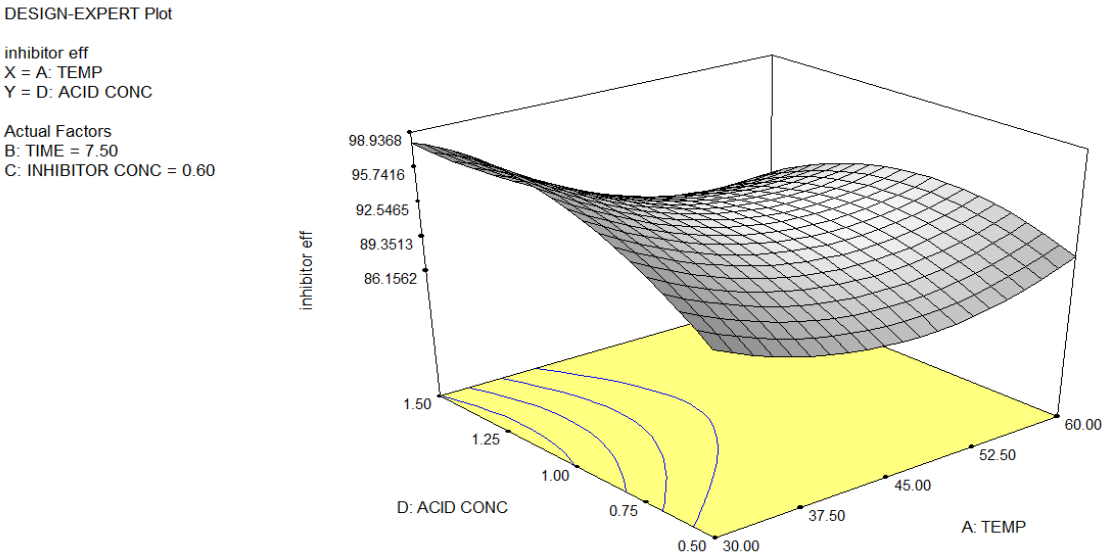

Figure 4.3b: 3-D model plot for inhibition efficiency of acid concentration versus temperature

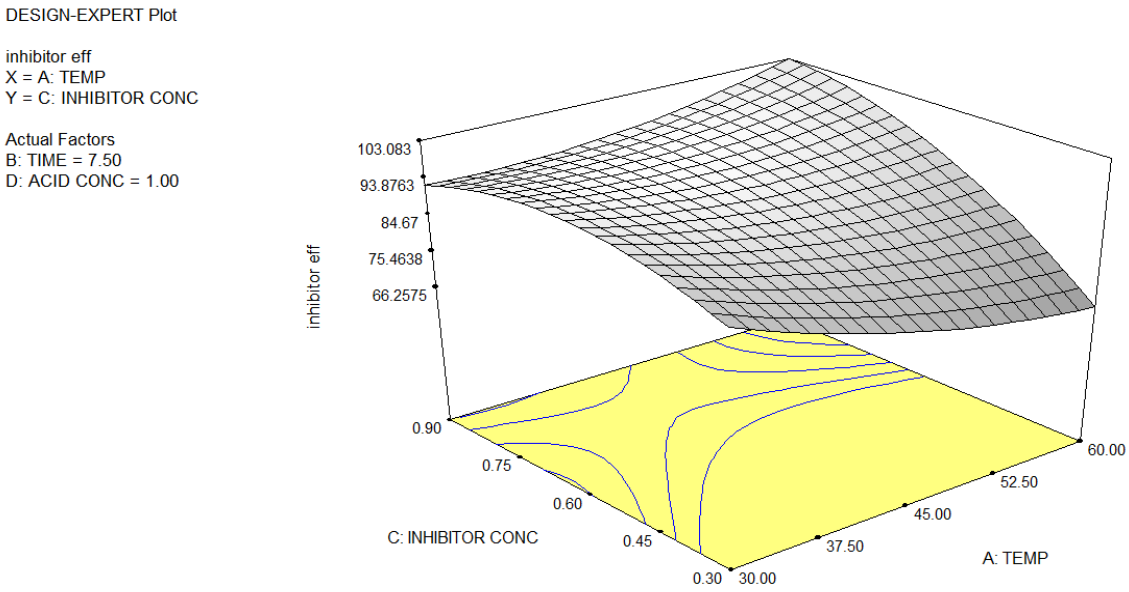

Figure 4.3c: 3-D model plot for inhibition efficiency of inhibitor concentration versus temperature

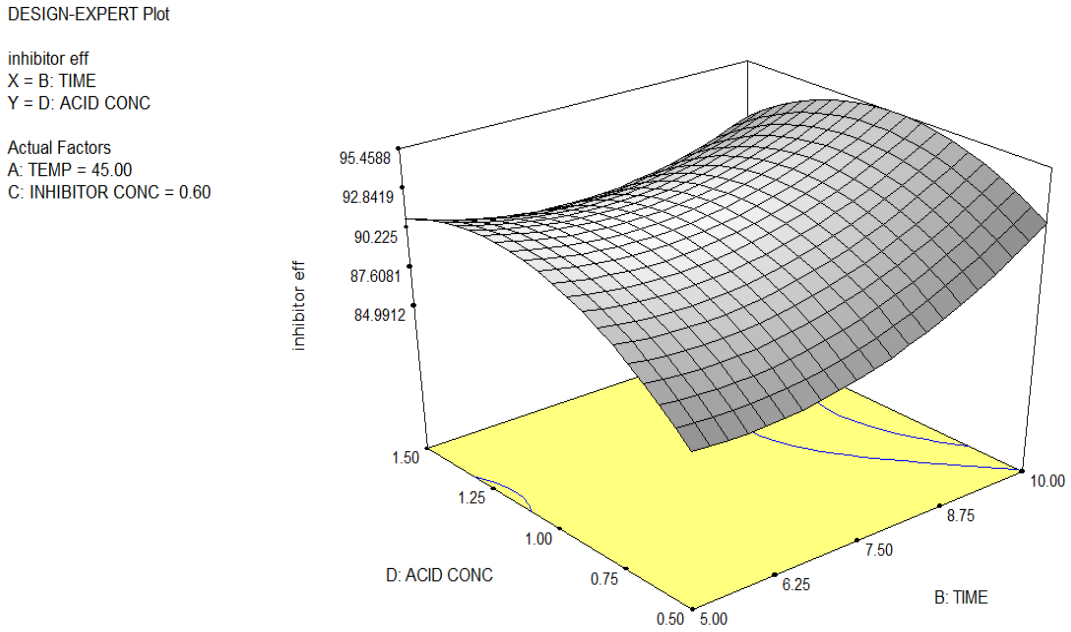

Figure 4.3d: 3-D model plot for inhibition efficiency of acid concentration versus immersion time

Figures 4.2d and 4.3d showed the impact of immersion period and acid concentration. Since the rate of corrosion and the binding of the IBLE to the metal surface are dependent on the immersion period and the acid concentration, the effects of immersion time and acid concentration are important. The increase of both variables caused a decrease in the inhibition efficiency. Inhibition efficiency is reached optimum value at low acid concentration.

4.4. Result for Statistical Analysis

4.4.1. ANOVA for Corrosion Rate

For the corrosion rate, the ANOVA for quadratic model showed an F-value of 7.18 and a Prob > F of below 0.0500, which indicated that the model terms are significant as shown in Table 4.4. The model terms are not significant if the values are greater than 0.05. Hence, C, D, C^2, AC and CD were acceptable model terms whereas, A, B, A^2, B^2, D^2, AB, AD, BC and BD were not acceptable. The inhibitor concentration had the highest F-value in the analysis of variance, accompanied by acid concentration, temperature, and immersion time. This indicated that inhibitor concentration, followed by acid concentration, temperature, and time, had the greatest impact on inhibition efficiency (Bas & Bayaci, 2007).

The regression equation for corrosion rate, formed in coded terms is as given in Equation 4.1. Table 4.4 shows the R^2 and adjusted R^2 values for corrosion rate. The R^2 and adjusted R^2 are 0.8777 and 0.7555, respectively. This demonstrated that the correlation coefficient and the adjusted correlation coefficient are in agreement. The adequate precision of 12.152 was obtained in Table 4.3 which suggested that the signal was sufficient.

Corrosion rate = +3.670E-004 + 1.439E-004A - 7.153E-005B - 4.746E-004C + 1.743E-004D - 1.561E-004 A^2 - 8.462E-005B^2 + 2.896E-004C^2 + 1.048E-004D^2 - 1.883E-005AB - 3.553E-004AC + 6.380E-005AD + 5.607E-005BC + 1.465E-005BD - 5.973E-004CD **Equation 4.1**

Where;

A = Temperature; B = Immersion time; C = Inhibitor concentration; D = Acid concentration.

Table 4.4: ANOVA result for corrosion rate (quadratic model)

Source	Sum of squares	*Df*	Mean Square	F-value	Prob > F	
Model	6.328E-006	14	4.520E-007	7.18	0.0004	Significant
A	2.485E-007	1	2.485E-007	3.95	0.0669	
B	6.140E-008	1	6.140E-008	0.98	0.3401	
C	2.072E-006	1	2.072E-006	42.92	< 0.0001	
D	3.647E-007	1	3.647E-007	5.79	0.0305	
A^2	1.580E-007	1	1.580E-007	2.51	0.1355	
B^2	4.644E-008	1	4.644E-008	0.74	0.4049	
C^2	5.439E-007	1	5.439E-007	8.64	0.0108	
D^2	7.122E-008	1	7.122E-008	1.13	0.3055	
AB	1.418E-009	1	1.418E-009	0.023	0.8829	
AC	5.050E-007	1	5.050E-007	8.02	0.0133	
AD	1.628E-008	1	1.628E-008	0.26	0.6190	
BC	1.258E-008	1	1.258E-008	0.20	0.6617	
BD	8.585E-010	1	8.585E-010	0.014	0.9087	
CD	1.427E-006	1	1.427E-006	22.67	0.0003	
Residual	8.815E-007	14	6.296E-008			
Lack of Fit	8.815E-007	10	8.815E-008			
Pure Error	0.000	4	0.000			
Cor Total	7.210E-006	28				
R^2	0.8777					
Adjusted R^2	0.7555					
Adequate Precision	12.152					

4.4.2. ANOVA for Inhibition Efficiency

Table 4.5 showed ANOVA results for the quadratic model of inhibition efficiency, where the F-value value of 6.60 and Prob > F of below 0.0500 indicated that the model terms were acceptable. Thus C, C^2, AC and CD were significant model terms while, A, B, D, A^2, B^2, D^2, AB, AD, BC and BD were not significant. The F-value for the inhibitor concentration was the largest in the analysis of variance, and then temperature, time, and acid concentration, which indicated that the inhibitor concentration mostly influenced the inhibition efficiency, accompanied by temperature, time, and acid concentration (Bas & Bayaci, 2007).

The regression equation for corrosion rate, formed in coded terms is as given in Equation 4.2. Table 4.5 showed the R^2 and adjusted R^2 values for inhibition effectiveness. The R^2 and adjusted R^2 are 0.8684 and 0.7368, respectively. This demonstrated that the correlation coefficient and the adjusted correlation coefficient are in agreement. Tables 4.4 revealed that the adequate precision was satisfactory, with a ratio of 10.628.

Inhibitor efficiency = +91.26 -3.03A +1.85B +9.95C +1.35D +3.75A^2 +2.35B^2 -7.31 C^2 -3.72D^2 +0.56AB +8.47AC -2.32AD -1.33BC -1.51BD +10.80CD **Equation 4.2**

Where;

A = Temperature; B = Immersion time; C = Inhibitor concentration; D = Acid concentration

4.5 Validation of the Optimal Process Level

The result of the optimal process level is as shown in Table 4.6. This was performed to validate the optimal process level of: temperature, time, inhibitor concentration and acid concentration of 38 °C, 5 days, 0.9 g/L and 1.0 M respectively, the inhibition efficiency obtained was 99.80 % which is in agreement with findings of Rashid & Khadom, (2019); Edoziuno *et al.,* (2020). The highest inhibition efficiency obtained from the experimental design is 99.6 %. This is significant to the inhibition efficiency obtained from the validated optimal process level due to the difference of 0.2 %.

Table 4.5: ANOVA result for inhibition efficiency (quadratic model)

Source	**Sum of squares**	***Df***	**Mean Square**	**F-value**	**Prob > F**	
Model	2823.69	14	201.69	6.60	0.0006	Significant
A	109.93	1	109.93	3.60	0.0787	
B	41.03	1	41.03	1.34	0.2660	
C	1186.84	1	1186.84	38.83	< 0.0001	
D	21.79	1	21.79	0.71	0.4127	
A^2	91.14	1	91.14	2.98	0.1062	
B^2	35.81	1	35.81	1.17	0.2974	
C^2	346.77	1	346.77	11.34	0.0046	
D^2	89.90	1	89.90	2.94	0.1084	
AB	1.23	1	1.23	0.040	0.8438	
AC	286.79	1	286.79	9.38	0.0084	
AD	21.48	1	21.48	0.70	0.4159	
BC	7.13	1	7.13	0.23	0.6366	
BD	9.09	1	9.09	0.30	0.5941	
CD	466.78	1	466.78	15.27	0.0016	
Residual	427.93	14	30.57			
Lack of Fit	427.93	10	42.79			
Pure Error	0.000	4	0.000			
Cor Total	3251.62	28				
R^2	0.8684					
Adjusted R^2	0.7368					
Adequate Precision	10.628					

Table 4.6: Validation of result for the optimal process level

S/n	Factor 1 A: Temperature (°C)	Factor 2 B: Immersion Time (days)	Factor 3 C: Inhibitor Conc (gL^{-1})	Factor 4 D: Acid Conc (M)	Response Inhibition Efficiency (%)	Surface coverage (ɵ)
1	38.0	5.0	0.9	1.0	99.80	0.9980

4.6. Results for Adsorption Isotherms and Thermodynamic studies

4.6.1. Result for Adsorption Isotherms

According to Znini *et al.,* (2012), Langmuir, Freundlich and Temkin are well-known isotherm models in which the fraction of the surface coverage is represented as a function of concentration and temperature. The values of correlation coefficient (R^2) and adsorption coefficient (K_{ads}) are shown in Table 4.7. The Langmuir isotherm provided the best fit, with R^2 varying from 0.9459 to 0.9993 at different temperatures.

The K_{ads} results (Table 4.7) revealed that as the temperature rose, the adsorption coefficient decreased. This indicated that IBLE adsorption on the substrate is more favourable at lower temperatures, which is in line with the inhibitory efficiency results. This supported what had been reported by Meroufel *et al.,* 2013; Hassan *et al.,* 2016; Wang *et al.,* 2019; Ogunleye *et al.,* 2020; and Lin *et al.,* 2021. The values of the correlation coefficient obtained at various temperatures for the Freundlich, Temkin, and Florry-Huggins isotherms are very low when compared to the Langmuir isotherm.

The negative ΔG_{ads} values observed in this investigation (Table 4.7) indicate that IBLE adsorption onto the mild steel surface is spontaneous and strong. An adsorption process is classified as physical adsorption when the value of ΔG_{ads} is around -20 kJ/mol, and chemical adsorption when it is around -40 kJ/mol. Physical and chemical adsorption mechanisms are both attributed to values within the range of the two limits (Meng *et al.,* 2016; Loto *et al.,* 2020; Lin *et al.,* 2021). The magnitude of ΔG_{ads} values, suggested that IBLE adsorbed on mild steel surface in H_3PO_4 via physisorption mechanism. The adsorption type and adsorption isotherm of natural corrosion inhibitors for steel in phosphoric acid are compared in Table 4.8.

4.6.2. Result for Thermodynamic study

The Arrhenius plot used to estimate the activation energy E_a of mild steel in H_3PO_4 in the presence of IBLE at various concentrations is shown in Figure 4.5. Physical adsorption is indicated by E_a < 80 kJ/mol, while chemical adsorption is indicated by E_a > 80 kJ/mol (Ogunleye *et al.,* 2020; Mohammed *et al.,* 2021; Gaber *et al.,* 2021). The attachment of IBLE molecules upon the steel surface followed a physical adsorption mechanism (Table 4.9).

Table 4.7: Result for Adsorption Isotherms

Isotherm	Temperature (^oC)	R^2	Slope	Intercept	K_{ads} (KJ/mol)	ΔG_{ads} (KJ/mol)
Langmuir	30	0.9993	0.9925	0.0208	48.08	-19.87
	45	0.9981	0.9175	0.1112	8.99	-16.42
	60	0.9459	0.7068	0.2541	3.94	-14.92
Freundlich	30	0.7177	0.0290	0.0065	1.02	-10.18
	45	0.9404	0.2086	0.0017	1.00	-10.63
	60	0.8840	0.4568	0.0411	1.10	-11.39
Temkin	30	0.7364	0.0288	0.9856	0.9856	-10.08
	45	0.9436	0.1803	0.9903	0.9903	-10.63
	60	0.8832	0.3595	1.0690	1.0690	-11.30
Flory-Huggin	30	0.6633	0.5432	1.1047	12.73	-16.53
	45	0.9737	0.5159	0.7375	5.46	-15.10
	60	0.7228	0.1680	0.3835	2.42	-13.57

Table 4.8: A comparison of natural inhibitors for mild steel with respect to adsorption type and adsorption isotherm in phosphoric acid

Metal	Inhibitor	Temperature	Adsorption type	Adsorption isotherm	R^2	References
Mild steel	l-Cysteine methyl ester hydrochloride	35 - 55 ^{o}C	Physical	Langmuir	0.99998	Zarrok *et al.,* 2014
Carbon steel	Alizarin red	25 ^{o}C	Comprehensive adsorption	Langmuir	0.99994	Ben Hmamou *et al.,* 2013
Mild steel	Hydrazine derivatives	35 ^{o}C	Comprehensive adsorption	Langmuir	1.00000	Belghiti *et al.,* (2016a, b)
Carbon steel	Guar gum	25 - 55 ^{o}C	Comprehensive adsorption	Temkin	0.99990	Messali *et al.,* 2017
Mild steel	*Ipomoea batatas* leaf	30 - 60 ^{o}C	Physical	Langmuir	0.99930	This research

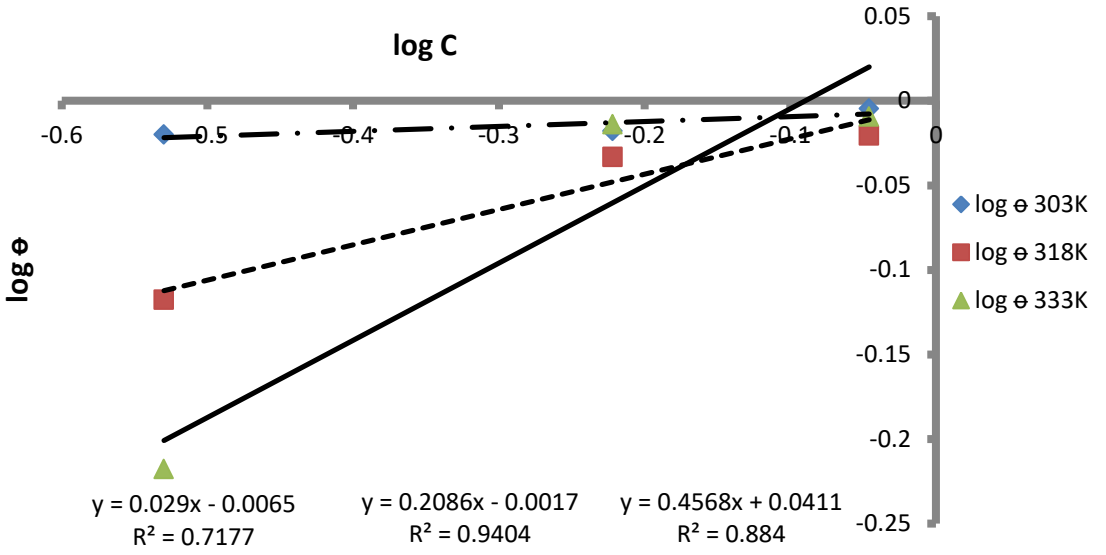

Figure 4.4a: Layout for Freundlich isotherm of mild steel in H_3PO_4

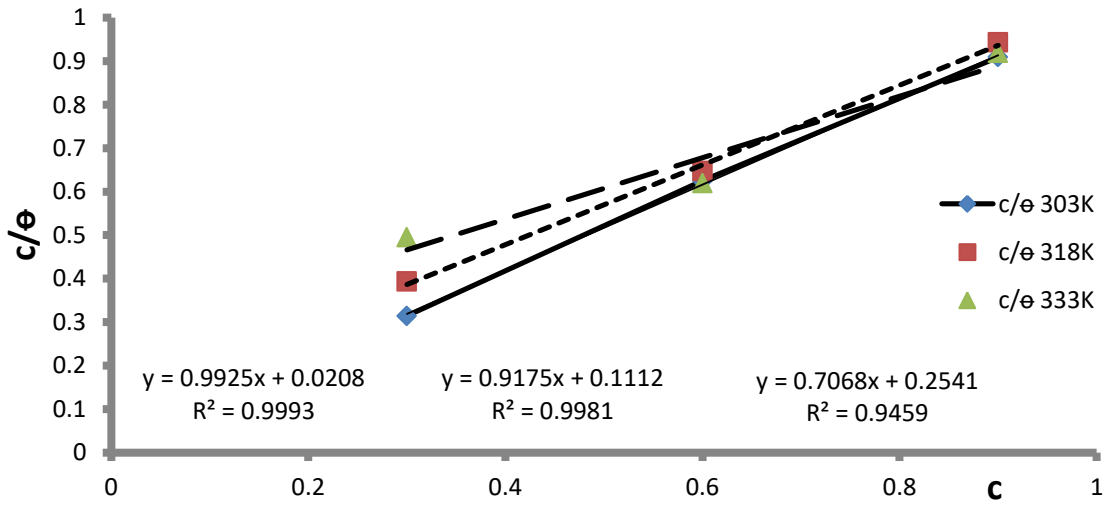

Figure 4.4b: Layout for Langmuir isotherm of mild steel in H_3PO_4

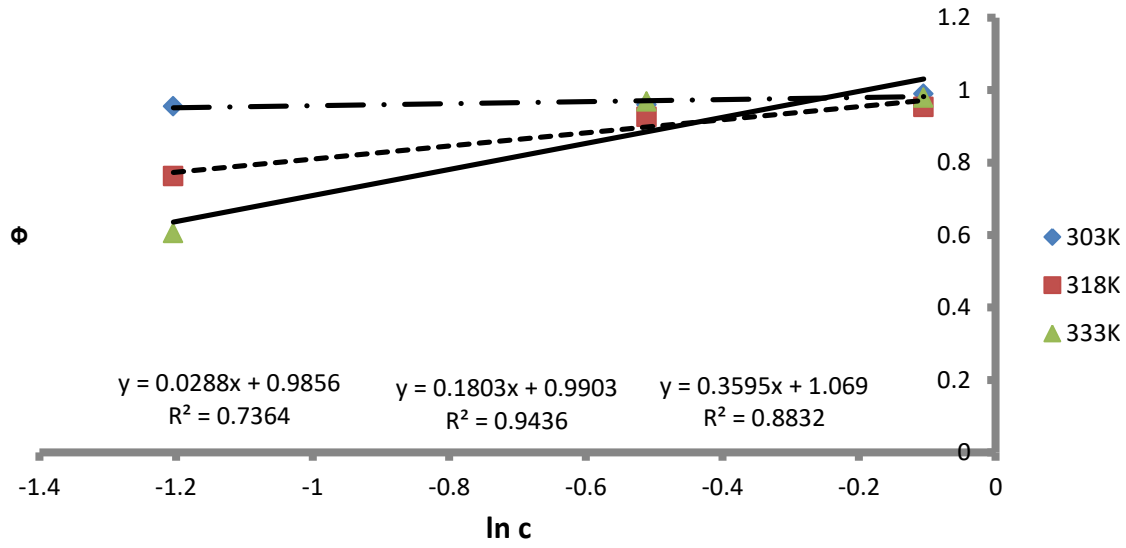

Figure 4.4c: Layout for Temkin isotherm of mild steel in H_3PO_4

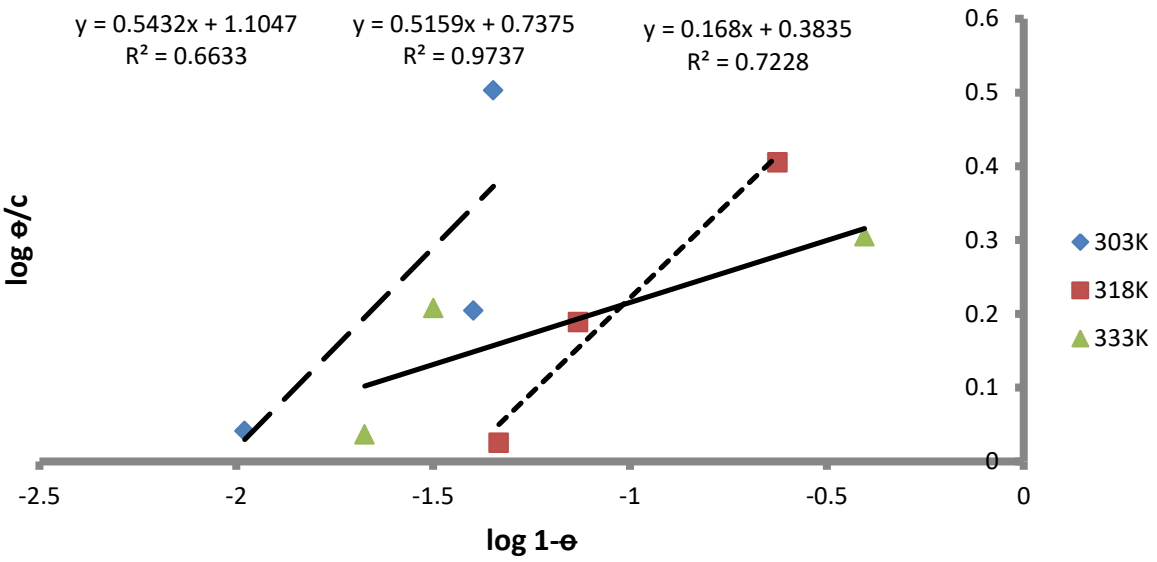

Figure 4.4d: Layout for Flory-Huggins isotherm of mild steel in H_3PO_4

Table 4.9: Enthalpy, Entropy and Activation Energy (ΔH_{ads}, ΔS_{ads} and E_a) values for the corrosion of mild steel in H_3PO_4 in the presence of IBLE

Concentration (g/L)	ΔH_{ads} (KJ/mol)			ΔS_{ads} (KJ/mol)			E_a (kJ/mol)		
	30 °C	45 °C	60 °C	30 °C	45 °C	60 °C	30 °C	45 °C	60 °C
0.3	12.2715	12.8790	13.4865	0.1061	0.0921	0.0853	18.159	19.058	19.957
0.6	15.7073	16.4811	17.2586	0.1174	0.1034	0.0966	8.422	8.339	9.256
0.9	28.9986	30.4342	31.8698	0.1613	0.1473	0.1405	6.492	6.812	7.134

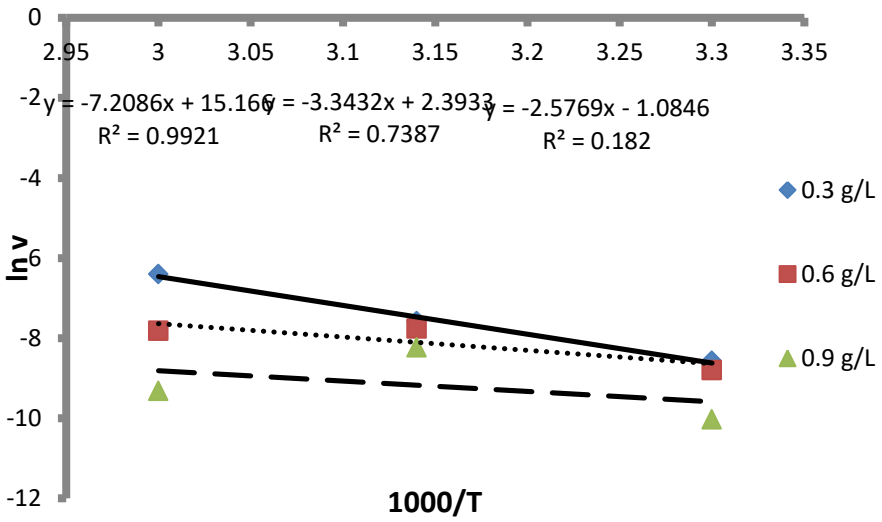

Figure 4.5a: Arrhenius plot for the corrosion of mild steel in H_3PO_4 in the presence of inhibitor

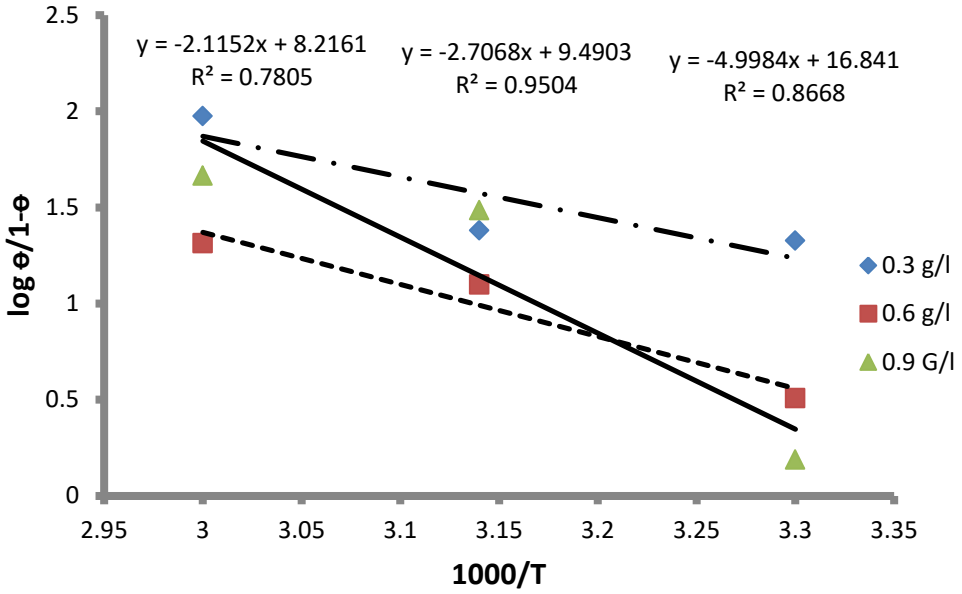

Figure 4.5b: Transition plot for the corrosion of mild steel in H_3PO_4 in the presence of inhibitor

The values of ΔH_{ads} are all positive indicating that the steel dissolution reaction in H_3PO_4 is an endothermic process while ΔH_{ads} values increased as shown in Table 4.9. The lower the IBLE concentration, the more the inhibitor molecules are physically adsorbed. They tend to undergo mixed adsorption, with physical adsorption dominating at greater IBLE concentrations (Lin *et al.,* 2021).

Due to the adsorption of the IBLE molecules onto the mild steel surface, the positive values of ΔS_{ads}, as shown in Table 4.9 indicated that the adsorption process caused an increase in the system's disorderliness (Obike *et al.,* 2018). The results of ΔH_{ads} and ΔS_{ads}, confirmed the results from Boudalia *et al.,* (2019); Chung *et al.,* (2020); Lin *et al.,* (2021).

4.7. Result for Kinetic Study

Table 4.10 displays the results obtained after fitting the data to the kinetic models chosen for this study, which include inhibition concentrations of 0.3–0.9 g/L, temperatures of 30 – 60 ^{o}C, and immersion times of 5 – 10 days (120–240 h). According to correlation coefficient (R^2 values) parameters, mild steel corrosion in the presence of IBLE followed zero-order kinetics, with high R^2 value of 0.8929. Figure 4.6 (a-i) depicts plots of WL versus t, ln WL versus t, and $\frac{1}{\mathrm{WL}}$ versus t, respectively. The results obtained are compatible with the report of Hassan *et al.,* 2016.

4.8. Results for Electrochemical Measurements

4.8.1. Electrochemical Impedance Spectroscopy (EIS)

Electrochemical impedance spectroscopy, commonly used to study corrosion behaviour was used, in this research. It was conducted at open circuit potential in inhibitor-free 1 M of H_3PO_4 and with various concentrations of IBLE. Figure 4.7a shows the Nyquist plot for mild steel in the presence and absence of various inhibitor concentrations, while Figure 4.7b shows the Bode plot for mild steel in the presence and absence of various inhibitor concentrations.

Table 4.10: Result for kinetic study of mild steel inhibition in H_3PO_4 in the presence of IBLE

Conditions	Zero Order		First Order		Second Order	
	K_0/hr	R^2	K_1/ hr	R^2	K_2/ hr	R^2
30 ^oC at 0.6 g/l	0.48	0.8929	-5.52	0.8811	19.13	0.8598
45 ^oC at 0.6 g/l	1.24	0.7500	-2.86	0.7500	8.47	0.7500
60 ^oC at 0.6 g/l	0.79	0.7500	-4.03	0.7500	11.56	0.7500

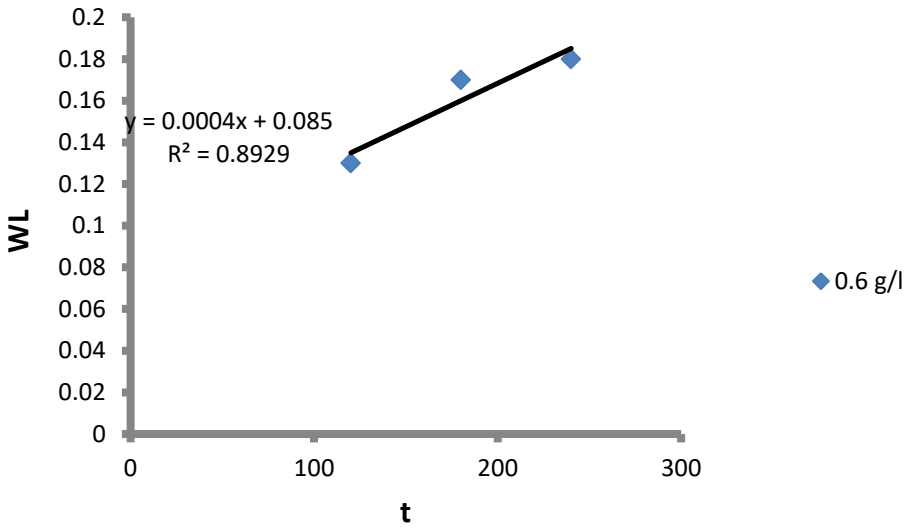

Figure 4.6(a): Layout for Pseudo-zero order kinetic model of mild steel in H_3PO_4 at 30 ^oC

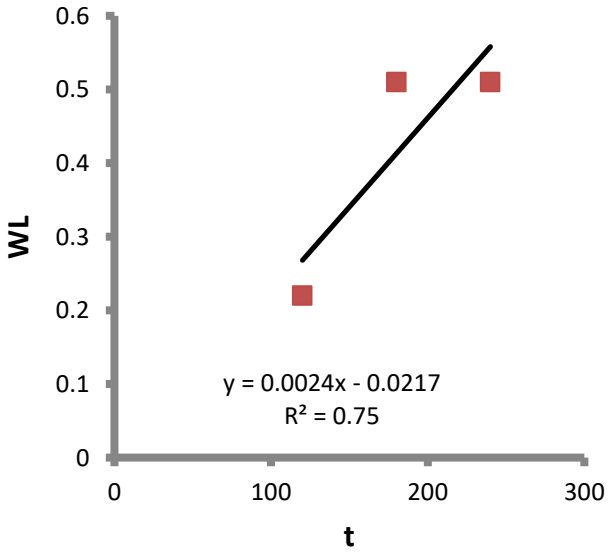

Figure 4.6(b): Layout for Pseudo-zero order kinetic model of mild steel in H_3PO_4 at 45 ^oC

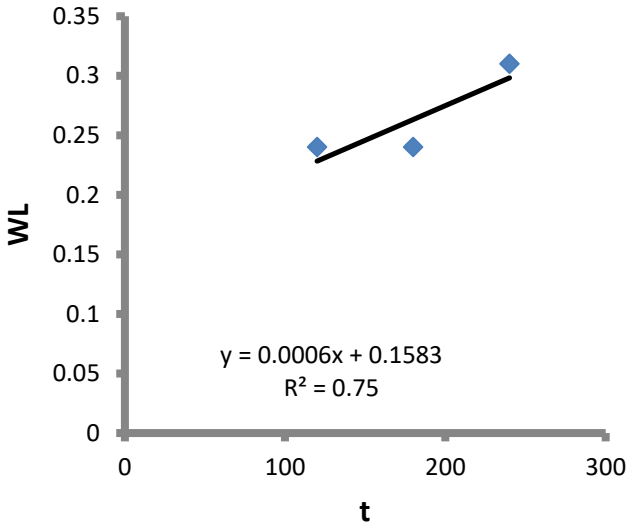

Figure 4.6(c): Layout for Pseudo-zero order kinetic model of mild steel in H_3PO_4 at 60 ^oC

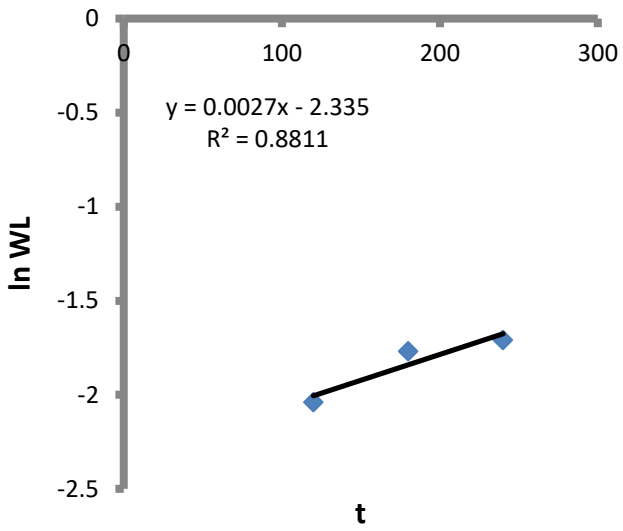

Figure 4.6(d): Layout for Pseudo-first order kinetic model of mild steel in H_3PO_4 at 30 ^oC

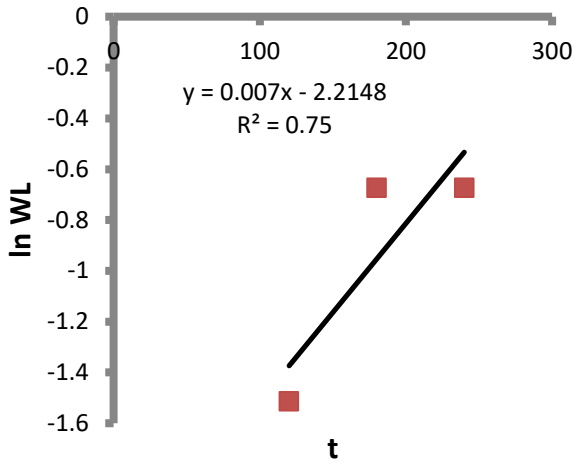

Figure 4.6(e): Layout for Pseudo-first order kinetic model of mild steel in H_3PO_4 at 45 ^oC

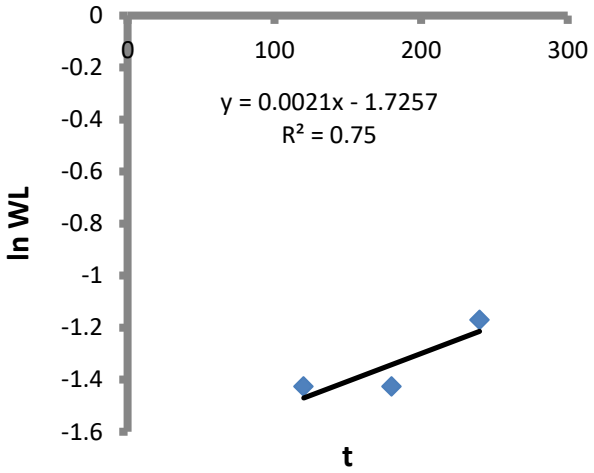

Figure 4.6(f): Layout for Pseudo-first order kinetic model of mild steel in H_3PO_4 at 60 ^oC

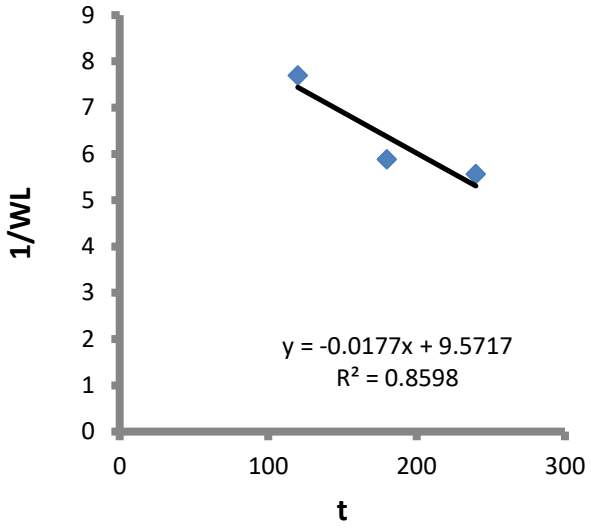

Figure 4.6(g): Layout for Pseudo-second order kinetic model of mild steel in H_3PO_4 at 30 ^oC

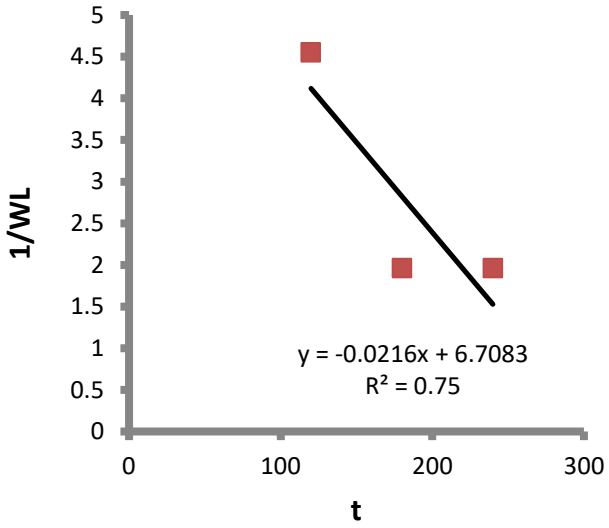

Figure 4.6(h): Layout for Pseudo-second order kinetic model of mild steel in H_3PO_4 at 45 ^oC

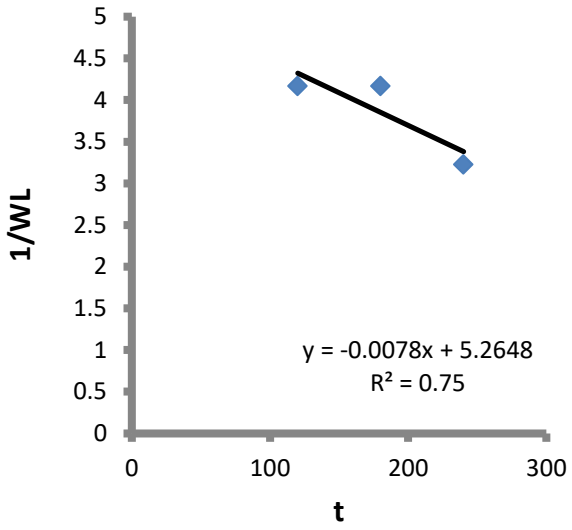

Figure 4.6(i): Layout for Pseudo-second order kinetic model of mild steel in H_3PO_4 at 60 ^oC

Table 4.11: Result for electrochemical impedance study for the corrosion control of mild steel in 1M H_3PO_4

Conc (gL^{-1})	Rs (Ω cm^2)	Rct (Ω cm^2)	CPE ($\mu Fcm^{-}N^2$)	N	IE (%)
Blank	1.7858	11.268	0.01614100	0.99827	-
0.3	2.6330	32.746	0.00003125	1.00040	65.59
0.6	2.7028	140.010	0.00013866	0.99572	91.95
0.9	3.4138	248.620	0.00011902	0.99507	95.47

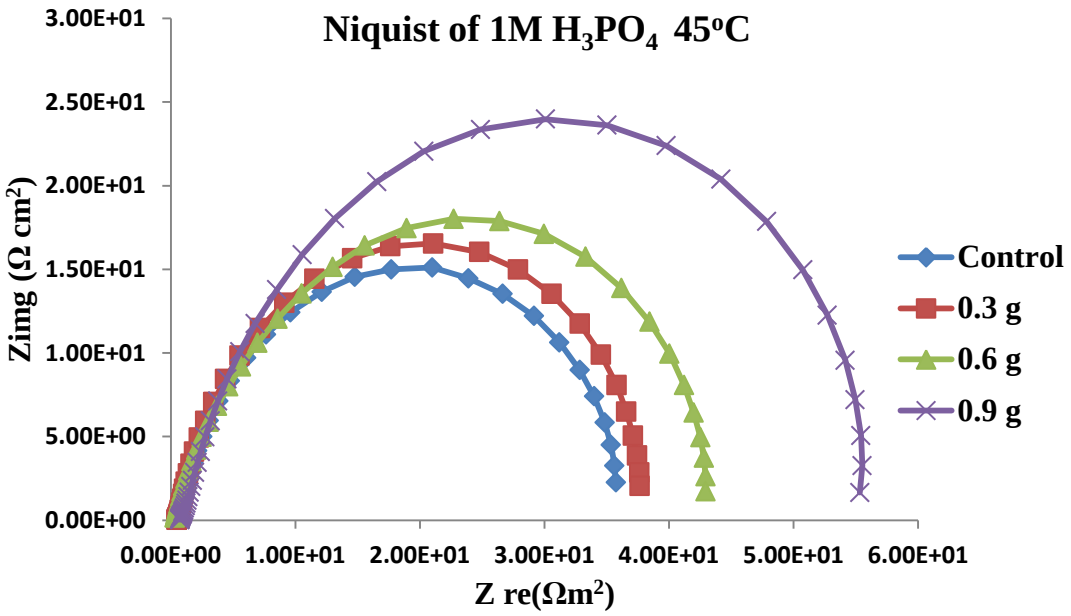

Figure 4.7a: Nyquist layout of mild steel in IBLE/H_3PO_4 medium

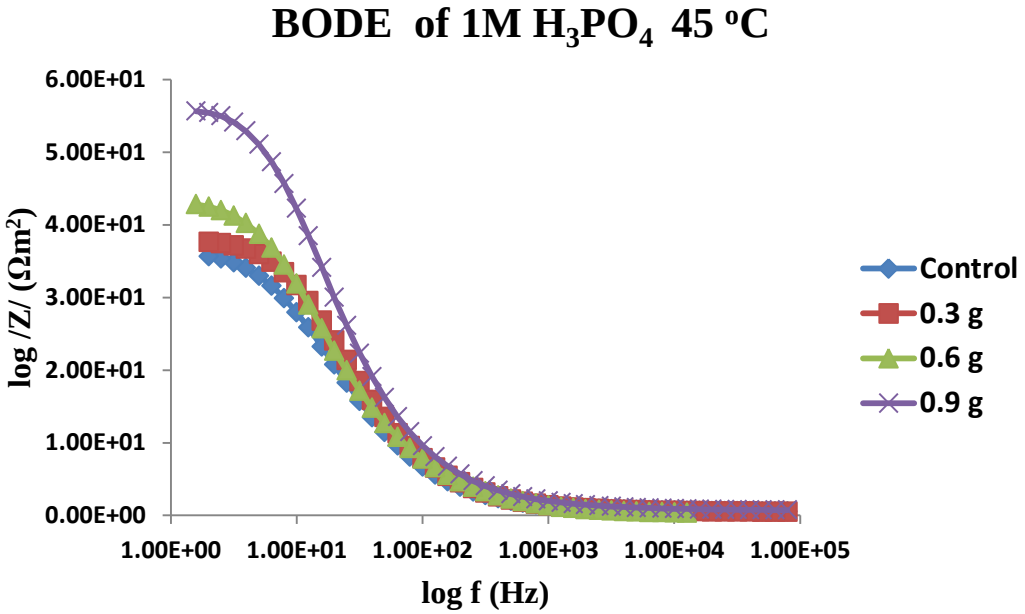

Figure 4.7b: BODE layout of mild steel in IBLE/H_3PO_4 medium

The diagram (Figure 4.7a) showed a depressed semicircle with single capacitive loop, which is attributed to charge transfer of the corrosion process. It is clear that the diameter of the semicircle increased with the increase in the inhibitor concentration in the electrolyte, indicating an increase in corrosion resistance of the material. Introducing IBLE increased the magnitude of the phase angles (values).

The impedance parameters (Table 4.11) show that the inhibitor containing solutions exhibited higher resistance (Rs) values than the blank. This agreed with the expected lower conductivity of the solution in the presence of organic compounds (Migahed *et al.,* 2016). The significant impedance or charge transfer resistance (Rct) values at increasing IBLE concentrations suggested that the inhibitors were reducing charge mobility in the electrochemical system (Mashuga *et al.,* 2017). Higher Rct values correspond to higher inhibition effectiveness, in other words, the inhibition efficiency increased as the inhibitor concentration was increased.

The highest impedance value was found for the optimum investigated inhibitor concentration of 0.9 g/L, reflecting the bio-active components of the extract which caused an increase in the surface coverage. The corrosion rate was inversely proportional to the charge transfer resistance (Rct), which reflected the degree of electron transport through the surface (Divya *et al.,* 2019). Rct values increased with increase in IBLE concentration in Table 4.11, which showed reduction in the rate of corrosion of the substrate and an increase in inhibition performance (Deyab & Guibal, 2020).

The values of absolute impedance at low frequency rise, with increase in inhibitor concentration as observed in the Figure 4.7b. This confirmed that the higher the concentration of IBLE, the higher the protection of mild steel in 1 M H_3PO_4 solution (Singh *et al.,* 2018). The constant phase element (CPE) was used in place of the double layer capacitance (Cdl) in these circuits to account for electrode surface heterogeneity caused via inhibitor adsorption, the formation of porous layers and thus to provide a more accurate fit to the experimental EIS data. The CPE values decreased as the inhibitor concentration in the acid solution increased, indicating that the inhibition efficiency improved. The decline in CPE values can be related to a reduction in the local dielectric constant because inhibitor molecules gradually replace water molecules that were originally adsorbed on the surface (Singh *et al.,* 2018).

In 1 M of H_3PO_4, the IBLE had an optimum inhibition performance of 95.47 %, as shown in Table 4.11. This suggested more inhibitor adsorption, which might be attributable to PO_4^{-1} ions' higher propensity to adsorb on the substrate. $PO4^{-1}$ ions performed a critical part in the inhibiting process by coupling adsorption on the substrate with IBLE. This result corroborated what had already been stated by Singh *et al.*, 2018 and Deyab & Guibal, 2020.

4.8.2. Potentiodynamic Polarization Studies

Figure 4.8 displays the tafel plot for mild steel corrosion at various concentrations. The linear sections of anode and cathode polarization curves were used to derive fundamental potentiodynamic parameters such as corrosion potential (Ecorr), anodic and cathodic Tafel slopes, and corrosion current density (Icorr).

Table 4.12 shows the estimated polarization values as well as the inhibition efficiency values for every concentration investigated. The presence of IBLE in the corrosive media (1M H_3PO_4) influenced anodic metallic dissolution and cathodic hydrogen elimination processes without altering the curves' similar features (Qiang *et al.,* 2018).

Furthermore, it is obvious that corrosion current density dropped considerably in the application of varied concentrations of IBLE, indicating that the ionic liquid molecules adsorb on the metallic surface (Verma *et al.*, 2018). The adsorption of IBLE on the metallic surface caused the active sites responsible for corrosive dissolution to become blocked, resulting in a decline in the values of corrosion current densities.

The application of H_3PO_4 considerably enhanced the corrosion potential (Ecoor), indicating anodic inhibition, as reported in Table 4.12 (Tsoeunyane *et al.,* 2019). Depending on the alterations within the Ecorr values of the inhibited metallic specimen in comparison to the Ecorr values of the uninhibited metallic specimen, ionic liquid substances studied can be categorized as anodic, cathodic, or the combination of both also known as mixed inhibitors.

Table 4.12: Result for potentiodynamic polarization for the corrosion control of mild steel in 1M H_3PO_4

Cs Conc (gL^{-1})	***-Ecorr*** **(v)**	***Icorr*** (A/cm^2)	**Ba (v/dec)**	**Bc (v/dec)**	**Rp (Ω)**	**CR (mm/yr)**	**IE (%)**
Blank	0.48754	0.0000269700	0.0036060	0.0046500	38.860	0.263740	-
0.3	0.47252	0.0000175810	0.0042657	0.0040495	51.317	0.204290	34.81
0.6	0.48211	0.0000105400	0.0037611	0.0044846	84.280	0.122470	60.92
0.9	0.47284	0.0000044007	0.0010822	0.0031251	179.384	0.051136	83.68

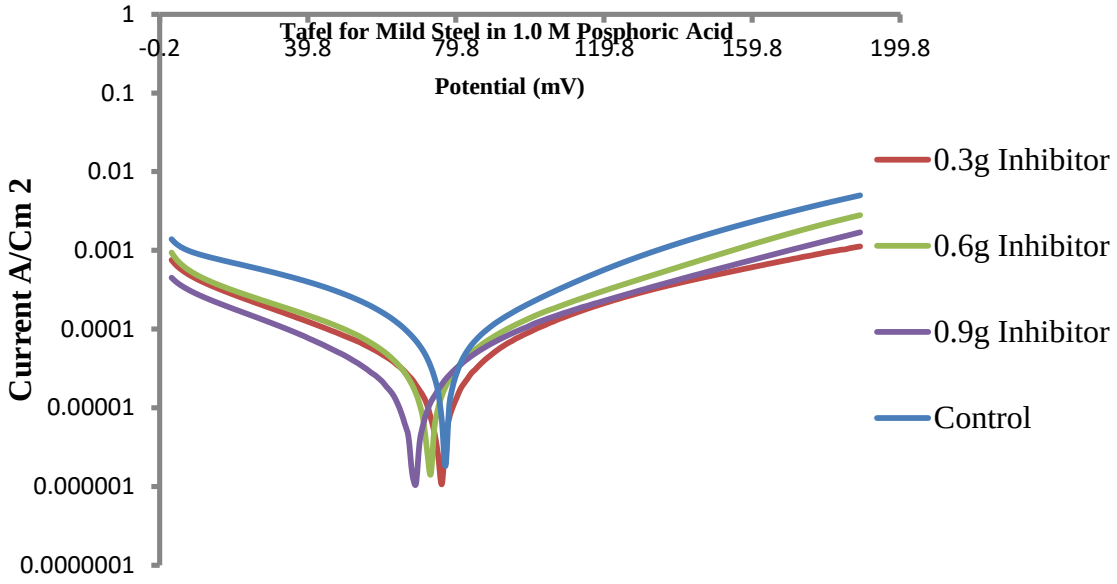

Figure 4.8: Tafel layout for mild steel in IBLE/H_3PO_4 mediu

If the difference in Ecorr values is greater than 85 mV, inhibitors are classified as cathodic or anodic, respectively; if the difference is less than 85 mV, inhibitors are classified as mixed (Verma, *et al.,* 2016). The displacement of Ecoor observed in Table 4.12, which is less than 85 mV, was used to deduce that IBLE behaved as a mixed-type inhibitor in this study.

4.9. Characterization and Metal Studies

4.9.1. Scanning Electron Microscopy (SEM)

The micrographs of the coupon immersed in H_3PO_4 without inhibitor (blank), the coupon with the highest inhibition efficiency from the experimental run, and the coupon from the validated experiment were examined using Scanning Electron Microscopy (SEM). Figure 4.9a showed a Scanning Electron Microscope of blank coupon. The surface morphology of the blank coupon and the coupon in the presence of inhibitor differed, as shown in Figure 4.9. In the absence of the extract, the blank coupon was severely damaged and corroded. Also, due to the lack of an inhibitor, pitting corrosion occurred in Figure 4.9a.

The coupon with the highest inhibition efficiency, had an outer layer formed on it by the extract, which acted as a shield, restricting the range of the acid's attack (Figure 4.9b). In addition, Figure 4.9c revealed that the coupon from the validated optimal process level had more protective film on its surface compared to the coupon with the highest inhibition efficiency (Figure 4.9b) as observed from the surface of the micrograph. This confirmed the results of Oyewole *et al.,* 2021.

4.9.2. Fourier Transform Infrared Spectrometer (FTIR)

Figure 4.10 (a-c) displays the FT-IR spectra FT-IR spectrum of the corrosion products of mild steel in the presence of H_3PO_4 (Blank), the corrosion products of mild steel in the presence of H_3PO_4 extract of *Ipomoea batatas* leaves at 45 ^oC (highest inhibition efficiency from experimental runs) and the corrosion products of mild steel in the presence of H_3PO_4 extract of *Ipomoea batatas* leaves at 38 ^oC (validated optimal process level). The respective peaks and functional groups of FT-IR are given in Table 4.13.

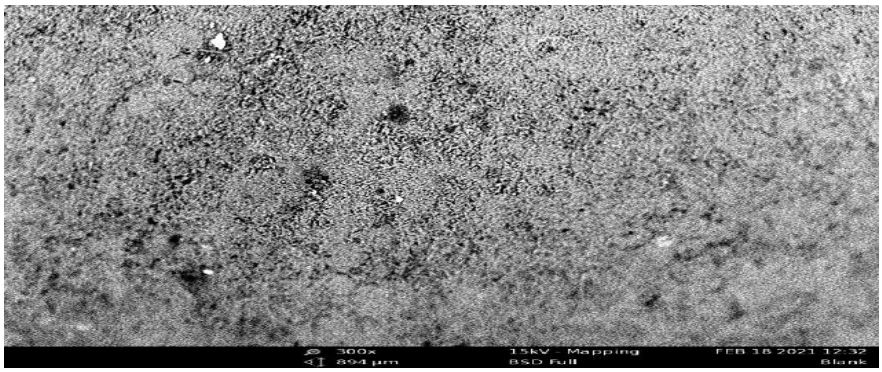

(a)

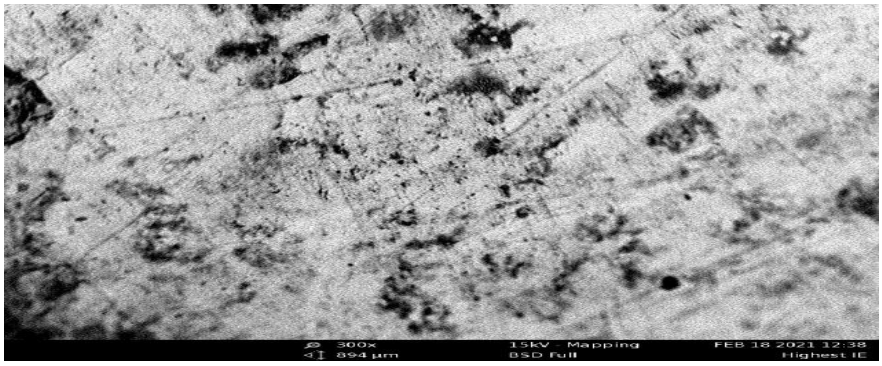

(b)

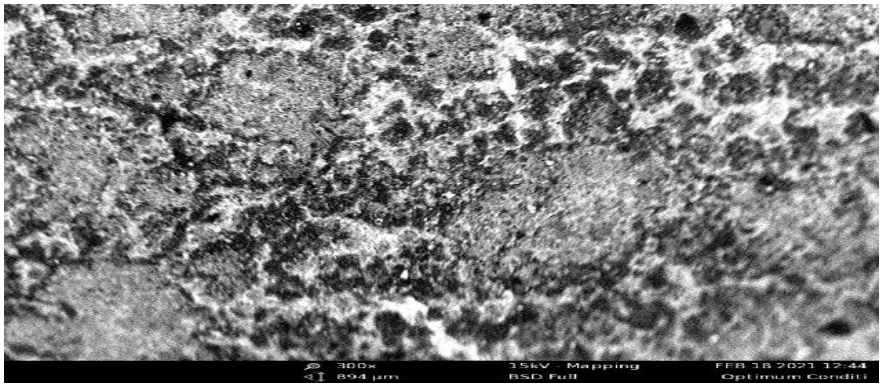

(c)

Figure 4.9 (a-c): SEM micrographs for the coupons (a) in 1 M H_3PO_4 solution at 45 ^oC (blank), (b) in 1 M H_3PO_4 solution at 45 ^oC with IBLE (highest inhibition efficiency from the experimental run), and (c) in 1 M H_3PO_4 solution at 38 ^oC with IBLE (validated experiment)

Table 4.13: Result of FTIR analysis showing peaks and assignment of the active components in the extract of the blank, highest inhibition efficiency and optimum condition respectively for the corrosion of mild steel

Run	Peak (Blank) (cm^{-1})	Peak (HIE) (cm^{-1})	Peak (VOPL) (cm^{-1})	Assignment (Blank)	Assignment (HIE)	Assignment (VOPL)
1	3582.74	3805.31	3998.26	O-H stretching vibration of the free hydroxyl-group of phenol	O-H stretching vibration	O-H stretching vibration
2	3122.40	3251.06	3308.41	C–H bond stretching vibration	O-H stretching vibration and N-H stretching vibration of amino acids	O-H stretching vibration
3	2598.51	3018.23	3199.74	C-H stretching vibration, of aliphatic Alkane	C-H stretching vibration	O-H stretching vibration of phenol groups,
4	2496.73	2639.73	3021.58	C-H stretching vibration	C-H stretching vibration	O-H stretching vibration
5	2296.43	1672.40	2999.58	CH_3 group stretching vibrations	C-O bending associated with OH group	C=O stretching vibrations
6	1750.64	1522.09	2982.55	C=O stretching vibration of a carbonyl bond	C=O stretching of aldehydes and ketones	C–H bond stretching vibrations
7	1398.41	1499.98	2843.62	O-H bending vibration of alcohol	CH_2 symmetric deformation	C-H stretching vibration
8	1200.08	1278.53	2228.71	C-O stretching	CH_2 symmetric	C=C-C aromatic ring stretch

Table 4.13: Result of FTIR analysis showing peaks and assignment of the active components in the extract of the blank, highest inhibition efficiency and optimum condition respectively for the corrosion of mild steel (Contd)

Run	Peak (Blank) (cm^{-1})	Peak (HIE) (cm^{-1})	Peak (VOPL) (cm^{-1})	Assignment (Blank)	Assignment (HIE)	Assignment (VOPL)
9	1126.28	1148.50	1400.97	C-N Stretching vibration	C - O - C asymmetric stretching vibration	CH_2 symmetric bending vibration
10	1000.73	1092.27	1200.04	C–O Stretching vibration of phenyl alkyl ether	stretching vibration of C-O, C-C and C-O-C anti-symmetric stretching vibration	C=O stretching vibrations
11	984.15	1019.66	1026.48	C-H Stretching vibration	C-OH stretching vibration	C–O Stretching vibration
12	862.40	890.11	898.27	C-O Stretching vibration of Akyl aryl ether	C-C Stretching vibration of alkenes	C-C Stretching vibration of amide group
13	800.24	698.71	800.00	CH bending vibration	C-Cl, Br, I Stretching vibration	CH bending vibration of alkenes

HIE - Highest inhibition efficiency
VOPL - Validated optimal process level

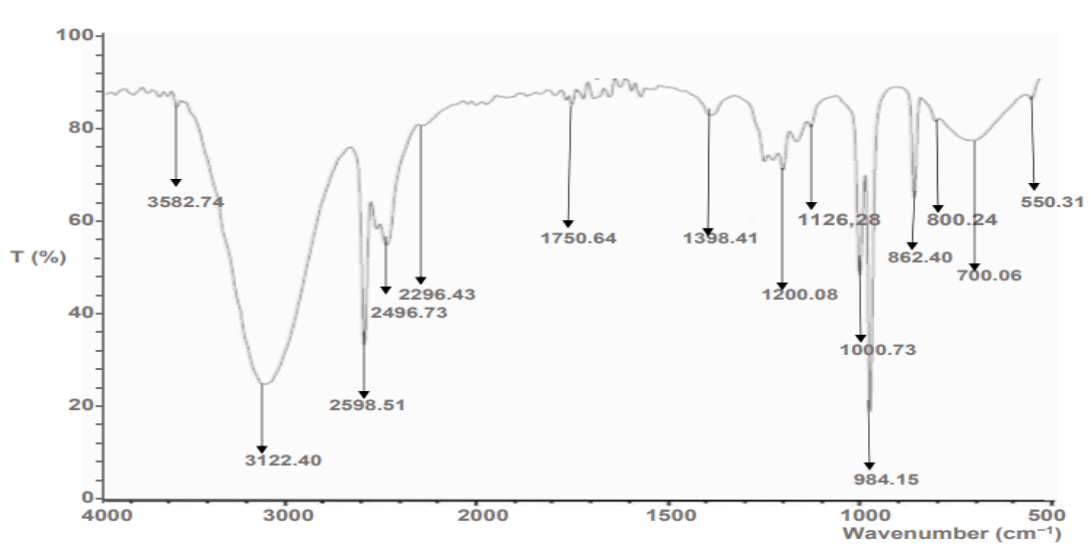

Figure 4.10a: FT-IR spectrum of the corrosion products of mild steel in H_3PO_4 at 45 ^oC (Blank)

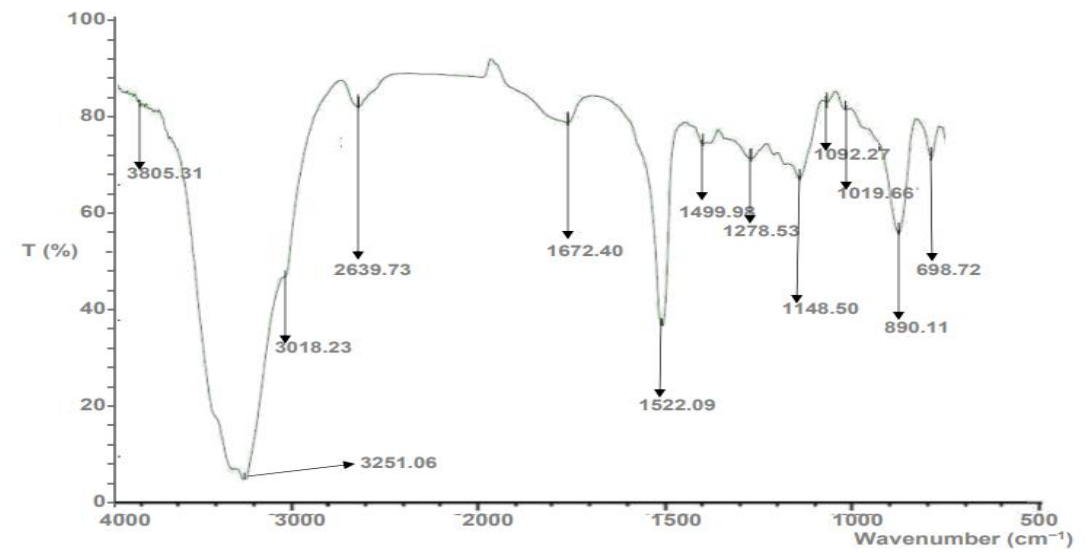

Figure 4.10b: FT-IR spectrum of the corrosion products of mild steel in the presence of H_3PO_4 extract of *Ipomoea batatas* leaves at 45 ^oC (highest inhibition efficiency from experimental runs)

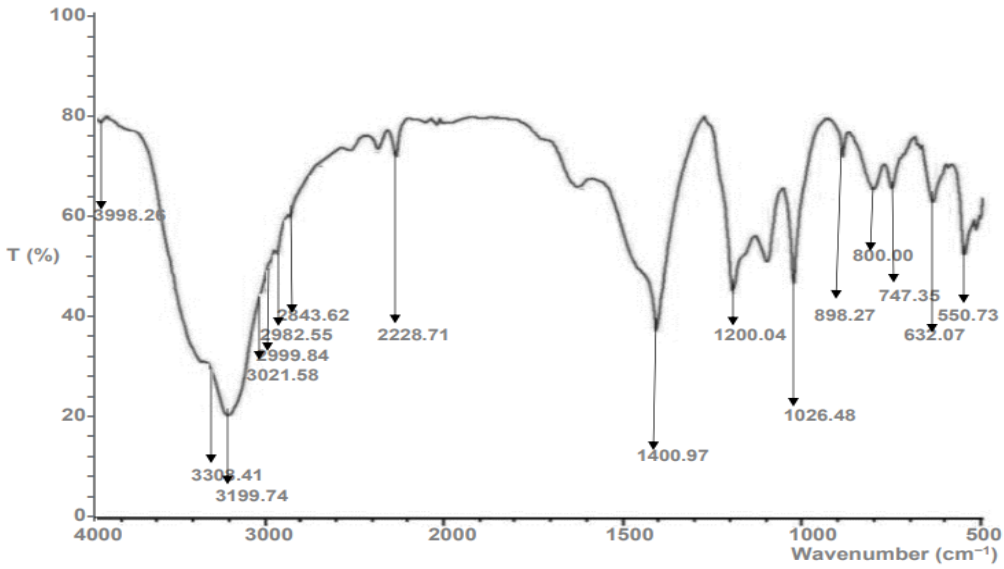

Figure 4.10c: FT-IR spectrum of the corrosion products of mild steel in the presence of H_3PO_4 extract of *Ipomoea batatas* leaves at 38 ^oC (validated optimal process level)

For the blank, peaks at 3582 and 2495.73 is attributed to O-H bond stretching vibration. The peaks at 3122.40, 2598.51 and 984.15 correspond to the stretching vibrations of C-H. The peak at 2598.51 indicates the presence of aliphatic or aromatic C-H groups. The stretching vibrations of CH_3 and C=O of a carbonyl bond, is observed at 2296.43 and 1750.64 respectively. The peaks at 1200 and 1126.28 correspond to the stretching vibrations of C-O and C-N respectively. The peak at 1398.41 is attributed to O-H bond bending vibration of alcohol.

The peak at 800.24 is assigned to the stretching vibrations of CH. 1000 and 862.40 correspond to the stretching vibrations of C-O in ethers.

The FT-IR peaks of IBLE were observed in the spectrum of inhibition efficiency (figure 4.10b). The peaks at 3805.03, 2639.73 and 3251.06 indicated O-H at stretching vibrations and N-H at stretching vibrations of amino acid, respectively. The bands at 3018, 1672.40 and 1522.09 is observed at stretching vibrations of C-H, C-O (OH group) and C=O (aldehydes and ketones), respectively. CH_2 symmetric deformation and scissoring, peaks at 1499.98 and 1278.53. Stretching vibrations of C-O-C (asymmetric); C-O, C-C, C-O-C (anti-asymmetric); C-OH; C-C (alkenes); C-Cl, Br, I; are observed at 1148.50, 1092.27, 1019.66, 890.11 and 698.71, respectively.

The FT-IR peaks of IBLE were observed in the spectrum of the validated optimal process level (figure 4.10c). The absorption bands at 3998.26, 3308.41, 3021.58 and 3199.74 can be attributed to O—H stretching vibrations. The stretching vibrations of C=O and C-H were observed in peaks of 2999.58, 1200.04; 2982.55, 2843.62, respectively. The peaks of 1400.97, 1026.48, 898.27 and 800 is due to the stretching vibrations of CH_2 (symmetric), C-O, C-C (amide group) and CH (alkene), respectively. According to Figure 4.13, the peaks of the highest inhibition efficiency and the validated optimal process level were higher than the blank. This research showed that the development of a thick barrier by the plant extract is responsible for mild steel corrosion prevention in H_3PO_4. The changes in absorption bands suggest that the adsorption between extract and coupon took place through these functional groups (Wang *et al.,* 2019; Hassan *et al.,* 2016). The results indicated that IBLE extract contained O, and N atoms such as O-H, C-O, C-N, C=O, C-H and aromatic structures that suit the basic requirements for a corrosion inhibitor and this confirmed what was reported by Olasehinde, 2018.

4.9.3. Energy Dispersive X-ray Fluorescence (EDXRF)

The EDXRF (Energy dispersive x-ray fluorescence) of the coupons in H_3PO_4 with and without inhibitor are presented Table 4.14. When compared to the coupon in the presence of IBLE at 45 ^oC (highest inhibition efficiency from the experimental run), the coupon in the H_3PO_4 at 45 ^oC solution (blank) displays a lower Fe content, revealing a low quantity of iron in the substrate.

Larger Fe band was found in the substrate immersed in H_3PO_4 solution with IBLE at 38 ^oC (validated experiment), revealing a slower amount of iron corrosion in the phosphoric acid.

These findings suggested that the presence of IBLE for the control of mild steel corroion in H_3PO_4 is responsible for the establishment of a barrier and validates what was previously reported by Prabakaran *et al.,* 2017 and Hemapriya *et al.,* 2017. Figure 4.11 (a-c) shows the EDXRF spectra of the blank coupon, the coupon of highest inhibition efficiency from the experimental runs and the coupon of validated optimal process level adsorbed on mild steel.

4.10. Mechanism of Inhibition

The corrosion inhibition mechanism was determined using the adsorption procedure as well as the composition of the elements in the IBLE. Compounds like O and N, contain heteroatoms over the mild steel, which supports their adsorptive property (Chung *et al.,* 2020). The functional groups (–NH, –C=O, –OH, –COOH) and other groups, as well as the availability of π electrons in the rings, were found to impede corrosion of mild steel using IBLE.

Previous study has indicated that several biomass materials, such as fruits, seeds, roots, leaves and barks as well as other bio-waste, such as citrus, tomato peels and peel of watermelon, are good corrosion inhibitors. Because of the amount of abundant organic molecules formed by sunlight, leaves were considered as excellent inhibitors (Sharma *et al.,* 2015; Prabakaran *et al.,* 2017; Hemapriya *et al.,* 2017; Verma *et al.,* 2018; Anitha *et al.,* 2019; Chung *et al.,* 2020).

In this study, IBLE was discovered to be a powerful mild steel corrosion inhibitor in H_3PO_4 medium. Through their heteroatoms, which act as polar functional substituents, aromatic and aliphatic heterocyclic rings, organic compounds in the

IBLE (phenols, tannins, steroids, glycosides, and saponins) are adsorbed to the mild steel surface.

The organic molecules in IBLE physically adsorbed onto the mild steel's surface, forming a protective coating that enabled anticorrosive capabilities and prevented acid attack.

Table 4.14: Result of EDXRF analysis showing elemental compositions of mild steel in 1 M H_3PO_4 at 45^oC solution (blank), in 1 M H_3PO_4 solution at 45^oC with IBLE (highest inhibition efficiency from the experimental run) and in 1 M H_3PO_4 solution at 38^oC with IBLE (validated experiment)

Element	Concentration % (Blank)	Concentration % (Highest inhibition efficiency)	Concentration % (Validated optimal process level)
Fe	18.960	25.318	29.814
Ni	0.00329	0.00207	0.00322
Cu	0.0191	0.0111	0.0369
Zn	0.00277	0.00387	0.00311
Ga	0.000549	0.000222	0.00026
Ge	0.000263	0	0.00031
Ta	0	0.0012	0
W	(-0.070)	(-0.060)	(-0.060)
Mg	0.07	0	0.28
Al	0.371	0.509	0.548
Si	0.5608	0.8854	0.9299
P	8.088	3.8534	1.7842
S	0.0739	0.0909	0.1733
Cl	0.186	0.275	0.394
K	0.0667	0.530	0.1078
Ca	0.0869	0.1392	0.1534
Ti	0.0100	0.0248	0.0188
V	0.01409	0.0199	0.0180
Cr	0.1192	0.1710	0.1965
Mn	0.3191	0.3916	0.4628
La	0.565	0.909	0.818
Ce	(-5.00)	(-10.00)	(-8.00)
As	0.0490	0.0198	0.0383
Br	0.000431	0.000171	0.000303

Table 4.14: Result of EDXRF analysis showing elemental compositions of mild steel in 1 M H_3PO_4 at 45^oC solution (blank), in 1 M H_3PO_4 solution at 45^oC with IBLE (highest inhibition efficiency from the experimental run) and in 1 M H_3PO_4 solution at 38^oC with IBLE (validated experiment) (Contd)

Element	Concentration % (Blank)	Concentration % (Highest inhibition efficiency)	Concentration % (Validated optimal process level)
Rb	0	0	0
Sr	(-1.0000)	(-1.0000)	(-1.0000)
Y	0	0.001151	0.001151
Zr	(-0.03000)	(-0)	(-0.03000)
Nb	0	0	0
Sn	0	1	0
Pb	1	1	1
Bi	0	0	0
Th	0	0	0
U	0	0	0
Ag	0	0	0
Sb	1	0	0
I	0	0	1
Cs	0	0	1
Ba	0	0	0

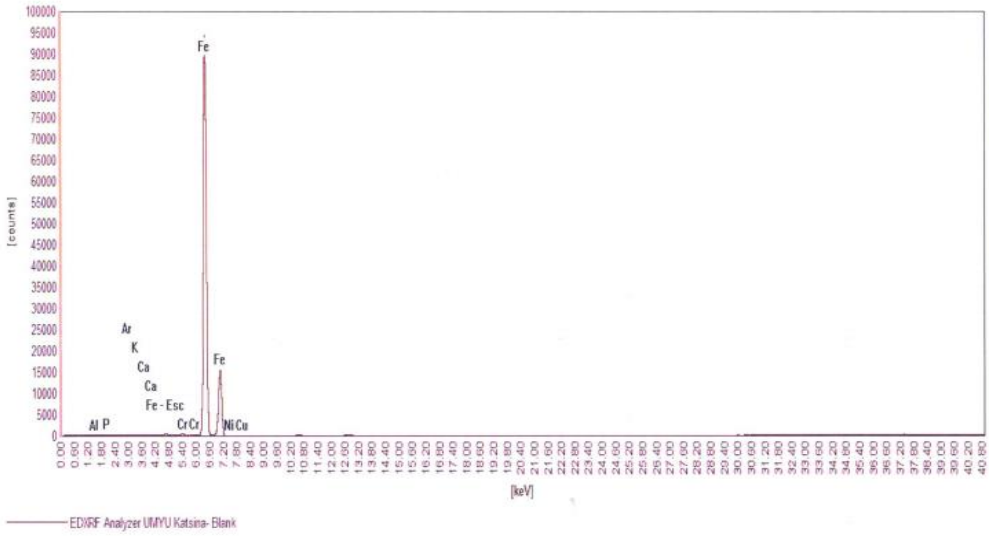

Figure 4.11a: EDXRF spectrum of the coupon in H_3PO_4 at 45 ^oC (blank)

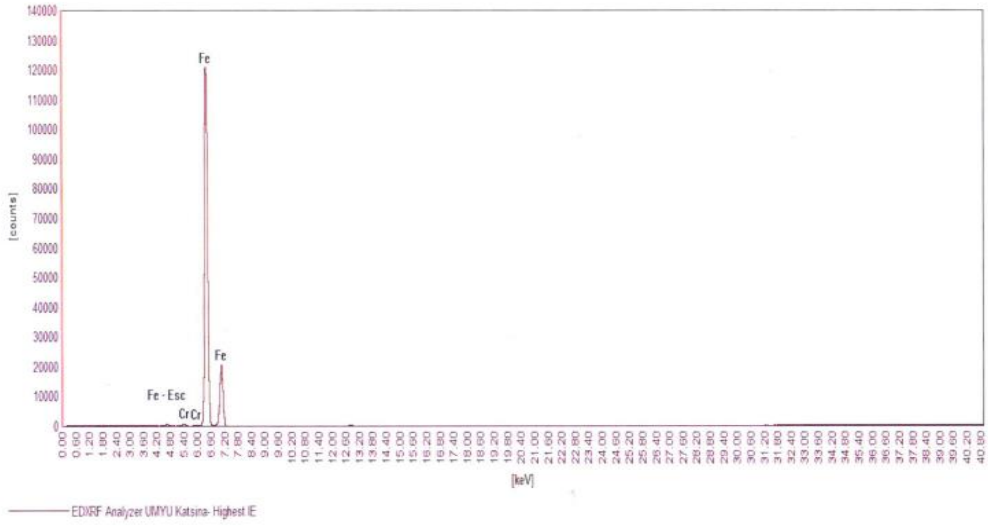

Figure 4.11b: EDXRF spectrum of the coupon in H_3PO_4 extract of *Ipomoea batatas* leaves at 45 ^oC (highest inhibition efficiency)

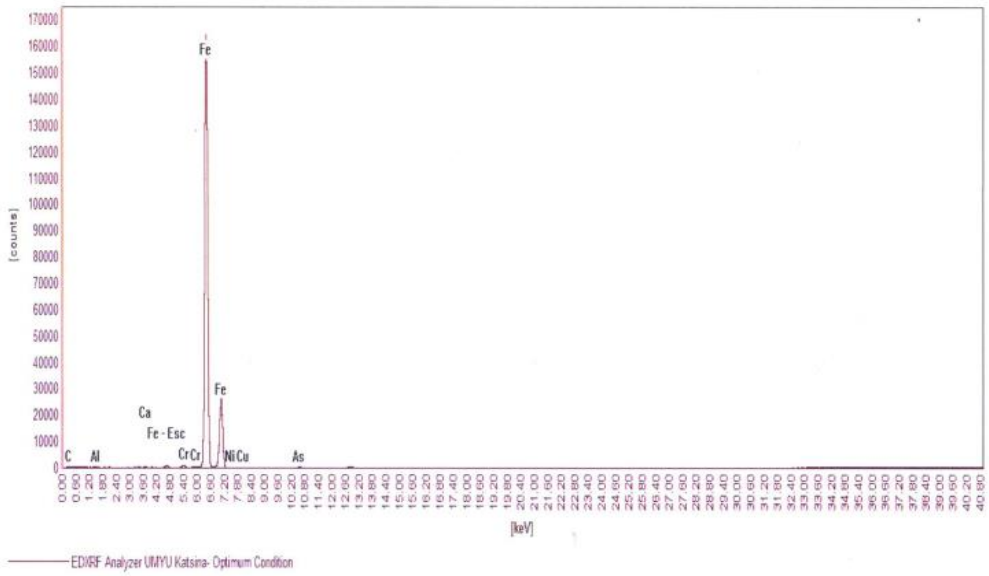

Figure 4.11c: EDXRF spectrum of the coupon in H_3PO_4 extract of *Ipomoea batatas* leaves at 38 ^oC (validated optimal process level)

CHAPTER FIVE

CONCLUSIONS AND RECOMMENDATIONS

5.1. Summary

Ipomoea batatas leaves extract (IBLE) was used as an ecologically acceptable inhibitor on mild steel in phosphoric acid environment. The phytochemical constituents present in IBLE which are responsible for its good inhibitory activities were tannins, phenol, saponins, steroids and glycosides. Optimization and kinetic studies were investigated with respect to the temperature (30 - 60 ^{o}C), immersion time (5 - 10 days), inhibitor concentration (0.3 - 0.9 g/L) and acid concentration (0.5 - 1.5 M). The rate of corrosion, inhibition efficiency, and surface coverage were all assessed.

5.2. Conclusions

The following conclusions were reached as a result of this study:

i. The phytochemical investigations showed that the extract (IBLE) contained phenols, saponins, tannins, glycosides, and steroids, making it an effective corrosion inhibitor.

ii. The result from the box Behnken design showed 99.6 % as the highest inhibition efficiency. The efficiency of inhibition rose as the extract concentration was increased. The optimal process level of IBLE at 0.9 g/L inhibitor concentration, immersion time of 5 days, acid concentration of 1.0 M and a temperature of 38 ^{o}C gave 99.8 % as its inhibition efficiency. The inhibition efficiencies of the electrochemical impedance spectroscopy and the potentiodynamic polarization were 95.45 % and 83.68 %, respectively. The weight loss analysis was in agreement with the electrochemical impedance spectroscopy. The result of the surface characterization showed that due to the presence of the extract, a protective film was formed which prevented the coupons from degrading.

iii. The inhibition of mild steel corrosion by IBLE followed the pseudo-zero order kinetic model. The adsorption properties of IBLE obeyed the Langmuir adsorption isotherm. E_a values obtained in presence of inhibitors were all below 80 kJ/mol indicating that the inhibition process was due to physical

adsorption. The values of ΔH_{ads} obtained indicated that the adsorption process were endothermic and spontaneous. The positive values of ΔS_{ads} indicated that there was an increase in the disorderliness of the system due to the adsorption of the IBLE molecules onto the mild steel surface.

5.3. Recommendations

Based on the research on corrosion behaviour of mild steel in H_3PO_4 using IBLE as corrosion inhibitor, the following recommendations are suggested:

i. Corrosion control of mild steel employing IBLE as a corrosion inhibitor in other acidic environments should be investigated.
ii. Further studies should be performed on corrosion control of other types of metals in other corrosion environment (alkaline).
iii. Other experimental designs should be used to undertake an optimization study on the influence of IBLE on mild steel dissolution.
iv. Further works should be conducted on the control of steel corrosion by mixing two or more different plant species as inhibitors.

REFERENCES

Abdelaziz, S., Benamira, M., Messaadia, L., Boughoues, Y., Lahmar, H., & Boudjerda, A., (2021) Green corrosion inhibition of mild steel in HCl medium using leaves extract of Arbutus unedo L. plant: An experimental and computational approach. *Colloids and Surfaces A: Physicochemical and Engineering Aspects*, 619: 126496. DOI: 10.1016/j.colsurfa.2021.126496.

Abou-Elseoud, W., Abdel-karim, A., Hassan, E., & Hassan, M., (2021) Enzyme- and acid-extracted sugar beet pectin as green corrosion inhibitors for mild steel in hydrochloric acid solution. *Carbohydrate Polymer Technologies and Applications*, 2: 100072. DOI: 10.1016/j.carpta.2021.100072.

Akalezi, C., Maduabuchi, A., Enenebeaku, C., & Oguzie, E., (2020) Experimental and DFT evaluation of adsorption and inhibitive properties of Moringa oliefera extract on mild steel corrosion in acidic media. *Arabian Journal of Chemistry*, 13(12): 9270-9282.

Akinbulumo, O. A., Odejobi, O. J., & Odekanle, E. L., (2020) Thermodynamics and Adsorption Study of the Corrosion Inhibition of Mild Steel by Euphorbia heterophylla L. Extract in 1.5 M HCl. *Results in Materials*, 5: 100074. DOI: 10.1016/j.rinma.2020.100074.

Alhassan A. S., & Abdulrazak B.A., (2020) Inhibition effect of ethanolic extract of ipomoea batatas peel on the corrosion of mild steel in hydrochloric acid medium. *Journal of Science and Mathematics Letters*, 8: 16-26.

Alibakhshi, E., Ramezanzadeh, M., Bahlakeh, G., Ramezanzadeh, B., M. Mahdavian & Motamedi, M., (2018) Glycyrrhiza glabra leaves extract as a green corrosion inhibitor for mild steel in 1 M hydrochloric acid solution: experimental, molecular dynamics, Monte Carlo and quantum. *Journal of Molecular Liquids*, 255: 185–198.

Alinnor, I., (2012) Corrosion Inhibition of Aluminium in Acidic Medium by Different Extracts of Ocimum gratissimum. *American Chemical Science Journal*, *2*(4): 122-135.

Alvarez P. E., Fiori-Bimbi M. V., Neske, A., Brandán, S. A., & Gervasi, C. A., (2018) Rollinia occidentalis extract as green corrosion inhibitor for carbon steel in HCl solution. *Journal of Industrial and Engineering Chemistry*, 58: 92-99.

Ammor, K., Bousta, D., Jennan, S., Bennani, B., Chaqroune, A., & Mahjoubi, F., (2018) Phytochemical Screening, Polyphenols Content, Antioxidant Power, and Antibacterial Activity of Herniaria hirsuta from Morocco. *The Scientific World Journal*, 2018: 1-7. doi: 10.1155/2018/7470384.

Anadebe, V. C., Onukwuli, O. D., Omotioma, M., & Okafor, N. A., (2019) Experimental, theoretical modeling and optimization of inhibition efficiency of pigeon pea leaf extract as anti-corrosion agent of mild steel in acid environment. *Materials Chemistry and Physics*, 233: 120-132.

Anitha, R., Chitra, S., Hemapriya, V., Chung, I., Kim, S., & Prabakaran, M., (2019) Implications of eco-addition inhibitor to mitigate corrosion in reinforced steel embedded in concrete. *Construction and Building Materials*, *213*: 246-256.

Ansari, K., Quraishi, M., & Singh, A., (2014) Schiff's base of pyridyl substituted triazoles as new and effective corrosion inhibitors for mild steel in hydrochloric acid solution. *Corrosion Science*, *79*: 5-15.

Aourabi, S., Driouch, M., Sfaira, M., Mahjoubi, F., Hammouti, B., Verma, C., Ebenso, E., & Guo, L., (2021) Phenolic fraction of Ammi visnaga extract as environmentally friendly antioxidant and corrosion inhibitor for mild steel in acidic medium. *Journal of Molecular Liquids*, 323: 114950. DOI: 10.1016/j.molliq.2020.114950.

Ayawei, N., Ebelegi, A. N., & Wankasi, D., (2017) Modelling and interpretation of adsorption isotherms. *Journal of Chemistry*, 2017, 1–11.

Balan, K. P., (2018). Corrosion. *Metallurgical Failure Analysis*, 155–178. doi:10.1016/b978-0-12-814336-0.

Bas, D., & Bayaci, I.H., (2007) Modelling and optimization I: usability of response surface methodology. *Journal of Food Engineering*, 78: 836-845.

Belghiti, M., Karzazi, Y., Tighadouini, S., Dafali, A., Jama, C., Warad, I., Hammouti, B., & Radi, S., (2016b) New hydrazine derivatives as corrosion for mild steel in phosphoric acid medium. Part B: Theoretical investigation. *Journal of Materials and Environment Science*, 7: 956–967.

Belghiti, M., Tighadouini, S., Karzazi, Y., Dafali, A., Hammouti, B., Radi, S., & Solmaz, R., (2016a) New hydrazine derivatives as corrosion inhibitors for mild steel protection in phosphoric acid medium. Part A: Experimental study. *Journal of Materials and Environment Science,* 7: 337–346.

Ben Harb, M., Abubshait, S., Etteyeb, N., Kamoun, M., & Dhouib, A., (2020) Olive leaf extract as a green corrosion inhibitor of reinforced concrete contaminated with seawater. *Arabian Journal of Chemistry,* 13: 4846–4856.

Ben Hmamou, D., Salghi, R., Zarrouk, A., Zarrok, H., Assouag, M., Hammouti, B., Al-Deyab, S., & Hezzat, M., (2013) Inhibition of carbon steel corrosion in phosphoric acid solution by Alizarin red. *Pharmacia Lettre,* 5: 135–142.

Bhuvaneswari, T. K., Vasantha, V. S., & Jeyaprabha, C., (2018) Pongamia Pinnata as a Green Corrosion Inhibitor for Mild Steel in 1N Sulfuric Acid Medium. *Silicon,* 10 (5): 1793-1807.

Boudalia, M., Fernández-Domene, R. M., Tabyaoui, M., Bellaouchou, A., Guenbour, A., & García-Antón, J., (2019) Green approach to corrosion inhibition of stainless steel in phosphoric acid of artemesia herba albamedium using plant extract. *Journal of Materials Research and Technology*, 8: 5763–5773.

Bupesh Raja, V., Palanikumar, K., Rohith Renish, R., Ganesh Babu, A., Varma, J., & Gopal, P. (2021). Corrosion resistance of corten steel – A review, *Materials Today: Proceedings*. DOI: 10.1016/j.matpr.2021.01.334.

Cai, J., Chen, C., Liu, J., & Liu, J., (2013) Corrosion resistance of carbon steel in simulated concrete pore solution in presence of 1-dihydroxyethylamino-3-dipropylamino-2-propanol as corrosion inhibitor. *Corrosion Engineering, Science and Technology*, 49(1): 66-72.

Chigondo, M., & Chigondo, F., (2016) Recent natural corrosion inhibitors for mild steel. *Journal of chemistry*, Article ID- 6208937: 1-7. doi.org/10.1155/2016/6208937.

Chung, I., Malathy, R., Priyadharshini, R., Hemapriya, V., Kim, S., & Prabakaran, M., (2020) Inhibition of mild steel corrosion using Magnolia kobus extract in sulphuric acid medium. *Materials Today Communications*, 25: 101687. DOI: 10.1016/j.mtcomm.2020.101687.

Chung, I.-M., Malathy, R., Kim, S.-H., Kalaiselvi, K., Prabakaran, M., & Gopiraman, M., (2020) Ecofriendly green inhibitor from Hemerocallis fulva against aluminum corrosion in sulphuric acid medium. *Journal of Adhesion Science and Technology*, 34(14): 1483-1506.

Dehghani, A., Bahlakeh, G., Ramezanzadeh, B., & Ramezanzadeh, M., (2020) Potential role of a novel green eco-friendly inhibitor in corrosion inhibition of mild steel in HCl solution: Detailed macro/micro-scale experimental and computational explorations. *Construction and Building Materials*, 245: 118464. DOI: 10.1016/j.conbuildmat.2020.118464.

Dehghani, A., Bahlakeh, G., Ramezanzadeh, B., hossein Mostafatabar, A. & Ramezanzadeh, M., (2020) Estimating the synergistic corrosion inhibition potency of (2-(3,4-)-3,5,7-trihydroxy-4H-chromen-4-one) and trivalent-cerium ions on mild steel in NaCl solution. *Construction and Building Materials*, 261: 119923. DOI: 10.1016/j.conbuildmat.2020.119923.

Deyab, M. A., & Guibal, E., (2020) Enhancement of corrosion resistance of the cooling systems in desalination plants by green inhibitor. *Scientific Reports*, 10(1): 4812. DOI: 10.1038/s41598-020-61810-9.

Divya, P., Subhashini, S., Prithiba, A., & Rajalakshmi, R., (2019) Tithonia Diversifolia flower Extract as green Corrosion Inhibitor for Mild Steel in Acid Medium. *Materials Today: Proceedings*, 18: 1581–1591.

Ebenso, E. E., Eddy, N. O., & Odongenyi, A. O., (2008) Corrosion Inhibitive Properties and Adsorption Behaviour of Ethanol Extract of Piperguinensis as a Green Corrosion Inhibitor for Mild Steel in H_2SO_4. *African Journal of Pure and Applied Chemistry*, 4: 107-115.

Edoziuno, F. O., Adediran, A. A., Odoni, B.U., Akinwekomi, A.D., Adesina O.S., & Oki M., (2020) Optimization and development of predictive models for the corrosion

inhibition of mild steel in sulphuric acid by methyl-5-benzoyl-2-benzimidazole carbamate (mebendazole). *Cogent Engineering*, 7:1, 1714100 doi.org/10.1080/23311916.2020.1714100.

Ejikeme, C. M., Ezeonu, C. S., & Eboatu, A. N., (2014) Determination of physical and phytochemical constituents of some tropical timbers indigenous to Niger Delta Area of Nigeria. *European Scientific Journal*, 10: 247–270.

Emembolu, L.N., Onukwuli, O.D., & Okafor, V.N., (2020) Characterization and Optimization study of Epiphyllum Oxypetalum extract as corrosion inhibitor for mild steel in 3M H_3PO_4 solutions. *World Scientific News*, 145: 256-273.

Emori, W., Zhanga, R., Okaforc, P. C., Zheng, X., He, T., Wei, K., Lina, X., & Cheng, C., (2020) Adsorption and corrosion inhibition performance of multi-phytoconstituents from Dioscorea septemloba on carbon steel in acidic media: Characterization, experimental and theoretical studies. *Colloids and Surfaces A*, 590: 124534. DOI: 10.1016/j.colsurfa.2020.124534.

Ezeonu, C., & Ejikeme, C. (2016). Qualitative and Quantitative Determination of Phytochemical Contents of Indigenous Nigerian Softwoods. *New Journal Of Science*, 1-9. doi: 10.1155/2016/5601327.

Faiz, M., Zahari, A., Awang, K., & Hussin, H., (2020) Corrosion inhibition on mild steel in 1 M HCl solution by Cryptocarya nigra extracts and three of its constituents (alkaloids). *RSC Advances*, 10(11): 6547–6562.

Farag, A., Ismail, A., & Migahed, M., (2018) Environmental-friendly shrimp waste protein corrosion inhibitor for carbon steel in 1 M HCl solution. *Egyptian Journal of Petroleum*, 27(4): 1187-1194.

Fayomi, O. S. I., Akande, I.G., & Odigie, S., (2020) Economic Impact of Corrosion in Oil Sectors and Prevention: An Overview. *Journal of Physics*: Conference Series 1378: 022037. DOI: 10.1088/1742-6596/1378/2/022037.

Foo, K. Y., & Hameed, B. H., (2010) Insight into the modelling of adsorption isotherms systems. *Chemical Engineering Journal*, 156: 2–10.

Fu, Q., Xu, J., Wei, B., Qin, Q., Gao, L., Bai, Y., Yu, C., & Sun, C., (2021) The effect of nitrate reducing bacteria on the corrosion behavior of X80 pipeline steel in the soil extract solution of Shenyang. *International Journal of Pressure Vessels and Piping*, 190: 104313. DOI: 10.1016/j.ijpvp.2021.104313.

Gaber, G., Ghobashy, M., Madani, M., Alshangiti, D., Alkhursani, S., Al-Gahtany, S., & Nady, N. (2021) Study of the corrosion-inhibiting activity of the green materials of the Posidonia oceanica leaves' ethanolic extract based on PVP in corrosive media (1 M of HCl). *Green Processing And Synthesis*, *10*(1), 555-568. doi: 10.1515/gps-2021-0055.

Gadow, H. S., & Motawea, M. M., (2017) Investigation of the corrosion inhibition of carbon steel in hydrochloric acid solution by using ginger roots extract. *RSC Advances,* 7(40): 24576–24588.

Garcés, P., Saura, P., Méndez, A., Zornoza, E., & Andrade, C., (2008) Effect of nitrite in corrosion of reinforcing steel in neutral and acid solutions simulating the electrolytic environments of micropores of concrete in the propagation period. *Corrosion Science*, *50*(2): 498-509.

Haldhar, R., Prasad D., & Bhardwaj, N., (2019) Extraction and experimental studies of *Citrus aurantifolia* as an economical and green corrosion inhibitor for mild steel in acidic media, *Journal of Adhesion Science and Technology*, 33(11): 1169-1183.

Hassan, K., Khadom, A., & Kurshed, N., (2016) Citrus aurantium leaves extracts as a sustainable corrosion inhibitor of mild steel in sulfuric acid. *South African Journal of Chemical Engineering*, *22*: 1-5.

Hemapriya, V., Prabakaran, M., & Parameswari, K., (2017) Experimental and theoretical studies on inhibition of benzothiazines against corrosion of mild steel in acidic medium. *Anti-Corrosion Methods and Materials*, 64: 306-314.

Hemapriya, V., Prabakaran, M., Parameswari, K., Chitra, S., Kim, S., & Chung, I., (2017) Experimental and theoretical studies on inhibition of benzothiazines against corrosion of mild steel in acidic medium. *Anti-Corrosion Methods and Materials*, *64*(3): 306-314.

Hou, B., Li, X., Ma, X., Du, C., Zhang, D., Zheng, M., Xu, W., Lu, D. & Ma, F., (2017). The cost of corrosion in China. *npj Materials Degradation*, 1(1). DOI: 10.1038/s41529-017-0005-2.

Hussain, M. I., Nawaz, S., Sajid, M. M., Nawaz, A., Irum, A., Javed, Y., & Yasin, G. (2020). Corrosion resistance of nanostructured metals and alloys. *Corrosion Protection at the Nanoscale, 63–87*. doi:10.1016/b978-0-12-819359-4.

Hussin, M. H., Jain Kassim, M., Razali, N. N., Dahon, N. H., & Nasshorudin, D., (2016) The effect of Tinospora crispa extracts as a natural mild steel corrosion inhibitor in 1M HCl solution. *Arabian Journal of Chemistry*, 9: S616–S624.

Hussin, M.H., & Kassim, M.J., (2011). The corrosion inhibition and adsorption behaviour of *Uncaria gambir* extract on mild steel in 1 M HCl. *Materials Chemistry* and *Physics*, 125: 461–468.

Khadom, A. A., Abdul, A. N., & Ahmed, N. A., (2018) *Xanthium strumarium* leaves extracts as a friendly corrosion inhibitor of low carbon steel in hydrochloric acid: Kinetics and mathematical studies. *South African Journal of Chemical Engineering*, 25: 13–21.

Khadom, A., & Abdul-Hadi, A., (2014) Kinetic and mathematical approaches to the corrosion of mild steel in nitric acid. *Reaction Kinetics, Mechanisms and Catalysis*, *112*(1): 15-26.

Krishnan, M., Subramanian, H., Dahms, H. U., Sivanandham, V., Seeni, P., & Gopalan, S., (2018) Biogenic corrosion inhibitor on mild steel protection in concentrated HCl medium. *Scientific Reports*, 8: 1-16.

Kumar, H., & Yadav, V., (2020) Musa acuminata (Green corrosion inhibitor) as anti-pit and anti-cracking agent for mild steel in 5M hydrochloric acid solution. *Chemical Data Collections*, 29: 100500. DOI: 10.1016/j.cdc.2020.100500.

Lee, H., Ryu, H., Park, W., & Ismail, M., (2015) Comparative Study on Corrosion Protection of Reinforcing Steel by Using Amino Alcohol and Lithium Nitrite Inhibitors. *Materials, 8*(1): 251-269.

Lin, B., Shao, J., Xu, Y., Lai, Y., & Zhao, Z., (2021) Adsorption and corrosion of renewable inhibitor of *Pomelo* peel extract for mild steel in phosphoric acid solution. *Arabian Journal of Chemistry*, 14(5): 103114. DOI: 10.1016/j.arabjc.2021.103114.

Liu, H., Gu, T., Zhang, G., Liu, H., & Cheng, Y., (2018) Corrosion of X80 pipeline steel under sulfate-reducing bacterium biofilms in simulated CO2-saturated oilfield produced water with carbon source starvation. *Corrosion Science,* 136: 47-59.

Liu, J., Chen, C., Cai, J., Liu, J., & Cui, G., (2012) 1,3-Bis-dibutylaminopropan-2-ol as inhibitor for reinforcement steel in chloride-contaminated simulated concrete pore solution. *Materials and Corrosion*, *64*(12): 1075-1081.

Loto, R. T., Fajobi, M., Oluwole, O., & Loto, C. A., (2020) Corrosion inhibition effect of calcium gluconate on mild steel in artificial seawater. *Cogent Engineering,* 7(1), 1712155. doi:10.1080/23311916.2020.17121.

Loto, R., Mbah, E. & Ugada, J., (2021) Corrosion inhibition effect of citrus sinensis essential oil extract on plain carbon steel in dilute acid media. *South African Journal of Chemical Engineering*, 35: 159-164.

Magrati, P., Subedi, D. B., Pokharel, D. B., & Bhattarai, J., (2020) Appraisal of Different Inorganic Inhibitors Action on the Corrosion Control Mechanism of Mild Steel in HNO_3 Solution. *Journal of Nepal Chemical Society,* 41(1): 64–73.

Mahross, M. H., Naggar, A.H., Seaf Elnasr, T. A., & Abdel-Hakim, M., (2016) Effect of Rice straw extract as an Environmental waste corrosion inhibitor on mild steel in acidic media. *Chemistry of Advanced Materials,* 1: 6-16.

Mashuga, M., Olasunkanmi, L. & Ebenso, E., (2017) Experimental and theoretical investigation of the inhibitory effect of new pyridazine derivatives for the corrosion of mild steel in 1 M HCl. *Journal of Molecular Structure,* 1136: 127-139.

Meng, Z. Hu, Y., Zhu, X. Ma, H., Li, J., Li, C., & Cao, D., (2016) Experimental and theoretical studies of benzothiazole derivatives as corrosion inhibitors for carbon steel in 1 M HCl. *Corrosion Science,* 112: 563–575.

Meroufel, B., Benali, O., Benyahia, M., Benmoussa, Y., & Zenasni, M.A., (2013) Adsorptive removal of anionic dye from aqueous solutions by mixture of Kaolin and Bentonite clay: Characteristics, isotherm, kinetic and thermodynamic studies. *Journal of Materials and Environmental Science,* 4(3): 482–491.

Messali, M., Lgaz, H., Dassanayake, R., Salghi, R., Jodeh, S., Abidi, N., & Hamed, O., (2017) Guar gum as efficient non-toxic inhibitor of carbon steel corrosion in phosphoric acid medium: electrochemical, surface, DFT and MD simulations studies. *Journal of Molecular Structure,* 1145: 43–54.

Migahed, M., Zaki, E. & Shaban, M., (2016) Corrosion control in the tubing steel of oil wells during matrix acidizing operations. *RSC Advances*, 6: 71384-71396.

Mobin, M., Basik, M., & Aslam, J., (2019) Pineapple stem extract (*Bromelain*) as an environmental friendly novel corrosion inhibitor for low carbon steel in 1 M HCl. *Measurement,* 134: 595–605.

Mohammed, N., Othman, N., Taib, M., Samat, M., & Yahya, S. (2021). Experimental and Theoretical Studies on Extract of Date Palm Seed as a Green Anti-Corrosion Agent in Hydrochloric Acid Solution. *Molecules*, *26*(12), 3535. doi: 10.3390/molecules26123535.

Moussout, H., Ahlafi, H., Aazza, M., & Maghat, H., (2018) Critical of linear and nonlinear equations of pseudo-first order and pseudo-second order kinetic models. *Karbala International Journal of Modern Science,* 4(2): 244–254.

Muthamma, K., Kumari, P., Lavanya, M., & Rao, S., (2020) Corrosion Inhibition of Mild Steel in Acidic Media by N-[(3,4-Dimethoxyphenyl)Methyleneamino]-4-Hydroxy-Benzamide. *Journal of Bio- and Tribo-Corrosion*, 7(1). DOI: 10.1007/s40735-020-00439-7.

Muthukumarasamy, K., Pitchai, S., Devarayan, K. & Nallathambi, L., (2020) Adsorption and corrosion inhibition performance of Tunbergia fragrans extract on mild steel in acid medium. *Materials Today: Proceedings*, 33: 4054-4058.

Nasab, S. G., Yazd, M. J., Semnani, A., Kahkesh, H., Rabiee, N., Rabiee, M., & Bagherzadeh, M., (2019) Natural Corrosion Inhibitors. *Synthesis Lectures on Mechanical Engineering,* 3(2): 1–96.

Noor, E., & Al-Moubaraki, A., (2008) Thermodynamic study of metal corrosion and inhibitor adsorption processes in mild steel/1-methyl-4[4′(-X)-styryl pyridinium iodides/hydrochloric acid systems. *Materials Chemistry and Physics*, 110(1): 145-154.

Noyel, V., Rohith, P., & Manivannan, R., (2015) Psidium guajava leaf extract as green corrosion inhibitor for mild steel in phosphoric acid. *International Journal of Electrochemical Science*, 10: 2220–2238.

Obike, A. I., Uwakwe, K. J., Ebeagwu, M. C., Okafor, P. C., & Ogili, E. C., (2018) Thermodynamic and Kinetic Studies of Powerful Eco Friendly Green Inhibitors; Costus afer, Uvaria chamae and Xylopia aethiopia for the Control of Mild Steel Corrosion in HCl Solution. *Journal of Physical Chemistry and Biophysics*, 8: 264. DOI: 10.4172/2161-0398.1000264.

Obike, A.I., Uwakwe, K.J., Abraham, E.K., Ikeuba, A.I., & Emori, W., (2020) Review of the losses and devastation caused by corrosion in the Nigeria oil industry for over 30 years. *International Journal of Corrosion and Scale Inhibition*, 9(1): 74-91.

Ogunleye, O. O., Arinkoola, A. O., Eletta, O. A., Agbede, O. O., Osho, Y. A., Morakinyo, A. F., & Hamed, J. O., (2020). Green corrosion inhibition and adsorption characteristics of Luffa cylindrica leaf extract on mild steel in hydrochloric acid environment. *Heliyon*, 6(1): e03205. DOI: 10.1016/j.heliyon.2020.e03205.

Ogwo, K., Osuwa, J., Udoinyang, I., & Nnanna, L., (2017) Corrosion Inhibition of Mild Steel and Aluminium in 1 M Hydrochloric Acid by Leaves Extracts of Ficus sycomorus. *Physical Science International Journal*, 14(3): 1-10.

Olasehinde, E. F., (2018) A Green Approach to Corrosion Mitigation of Mild Steel in Acid Medium Using Caesapinia Bonduc Seed Coat Extract. *FUTA Journal of Research in Sciences*, 14(1): 12-26.

Olawale, O., Adediran, A., Oyinbo, T., & Kalawole, O., (2017) Inhibitory action of rice husk extract (RHE) on the corrosion of carbon steel in acidic media. *Aceh International Journal of Science and Technology*, 6(2): 44-51.

Olawale, O., Bello, J. O., Ogunsemi, B. T., Uchella, U. C., Oluyori, A. P., & Oladejo, N. K. (2019). Optimization of chicken nail extracts as corrosion inhibitor on mild steel in 2M H2SO4. *Heliyon*, 5(11): e02821. DOI: 10.1016/j.heliyon.2019.e02821.

Olawale, O., Bello, J.O., & Akinbami P., (2015) A Study on Corrosion Inhibitor of Mild-Steel in Hydrochloric Acid using Cashew Waste. *International Journal of Modern Engineering Research*, 5: 25-30.

Oyewole, O., Oshin, T. A., & Atotuoma, B. O., (2021) Corchorus olitorius stem as corrosion inhibitor on mild steel in sulphuric acid. *Heliyon*, 7(4): *e06840.* doi:10.1016/j.heliyon.2021.e068.

Prabakaran, M., Kim, S. H., Sasireka, A., Kalaiselvi, K., & Chung, I. M., (2018) Polygonatum odaratum extract as an eco-friendly inhibitor for aluminum corrosion in acidic medium. *Journal of Adhesion Science and Technology*, 32(18): 2054-2069.

Prabakaran, M., Kim, S., Oh, Y., Raj, V., & Chung, I., (2017). Anticorrosion properties of momilactone A isolated from rice hulls. *Journal of Industrial and Engineering Chemistry*, 45: 380-386.

Prabakaran, M., Kim, S.H., & Sasireka, A., (2017) β-Sitosterol isolated from rice hulls as an efficient corrosion inhibitor for mild steel in acidic environments. *New Journal of Chemistry*, 41: 3900-3907.

Pradeep Kumar, C. B., & Mohama, K. N., (2014) Phytochemical Screening and Corrosion inhibitive behaviour of *petroleum hexapetalum* and *celosia argentea* plant extracts on mild steel in industrial water medium. *Egyptian Journal of Petroleum*, 23: 201-211.

Qiang, Y., Zhang, S., Tan, B., & Chen, S., (2018) Evaluation of Ginkgo leaf extract as an eco-friendly corrosion inhibitor of X70 steel in HCl solution. *Corrosion Science*, 133: 6-16.

Rajabipour, A., & Melchers, R., (2013) A numerical study of damage caused by combined pitting corrosion and axial stress in steel pipes. *Corrosion Science*, 76: 292-301.

Rashid, K.H., & Khadom, A.A., (2019) Optimization of inhibitive action of sodium molybdate (VI) for corrosion of carbon steel in saline water using response surface methodology. *Korean Journal of Chemical Engineering* 36: 1350–1359. https://doi.org/10.1007/s11814-019-0291-1.

Sachan, R. & Singh, A., (2020). Comparison of microbial influenced corrosion in presence of iron oxidizing bacteria (strains DASEWM1 and DASEWM2). *Construction and Building Materials*, 256: 119438. DOI: 10.1016/j.conbuildmat.2020.119438.

Saxena, A., Prasad, D., Haldhar, R., Singh, G., & Kumar, A., (2018). Use of Saracaashoka extract as green corrosion inhibitor for mild steel in 0.5 M H_2SO_4. *Journal of Molecular Liquids,* 258: 89–97.

Sharma, S., Peter, A., & Obot, I., (2015) Potential of Azadirachta indica as a green corrosion inhibitor against mild steel, aluminum, and tin: a review. *Journal of Analytical Science and Technology*, *6*(1). DOI: 10.1186/s40543-015-0067-0.

Shreir, L. L., (2010) Basic concepts of corrosion. *Article on Corrosion Science,* 1:3-15.

Simmons, C. H., Maguire, D., E., & Phelps, N., (2020) Surface finish and corrosion of metals. *Manual of Engineering Drawing,* 2020, 383–393.

Singh, A., Ebenso, E., & Quraishi, M., (2012) Corrosion Inhibition of Carbon Steel in HCl Solution by Some Plant Extracts. *International Journal of Corrosion*, *2012*, 1-20.

Singh, A., Samih Mohamed, H., Singh, S., Yu, H. & Lin, Y., (2020) Corrosion inhibition using guar gum grafted 2-acrylamido-2-methylpropanesulfonic acid (GG-AMPS) in tubular steel joints. *Construction and Building Materials*, 258: 119728. DOI: 10.1016/j.conbuildmat.2020.119728.

Singh, D., Ebenso, E., Singh, M., Behera, D., Udayabhanu, G. & John, R., (2018) Non-toxic Schiff bases as efficient corrosion inhibitors for mild steel in 1 M HCl: Electrochemical, AFM, FE-SEM and theoretical studies. *Journal of Molecular Liquids,* 250: 88-99.

Sivaraju, M., & Kannan, K., (2010) Inhibitive properties of plant extract (*Acalypha indica* L.) on mild steel corrosion in 1 N phosphoric acid. *International Journal of ChemTech Research,* 2: 1243–1253.

Soufeiani, L., Foliente, G., Nguyen, K., & San Nicolas, R., (2020) Corrosion protection of steel elements in façade systems- A review. *Journal of Building Engineering*, 32: 101759. DOI: 10.1016/j.jobe.2020.101759.

Tanzi, M. C., Farè, S., & Candiani, G. (2019). Sterilization and Degradation. *Foundations of Biomaterials Engineering, 289–328.* doi:10.1016/b978-0-08-101034-1.

Umoren, S. A., Solomon, M. M., Obot, I. B., & Sulieman, R. K., (2019) A critical review on the recent studies on plant biomaterials as corrosion inhibitors for industrial metals, *Journal of Industrial and Engineering Chemistry,* 76: 91–115.

Umoren, S., Eduok, U., Israel, A., Obot, I., & Solomon, M., (2012) Coconut coir dust extract: a novel eco-friendly corrosion inhibitor for Al in HCl solutions. *Green Chemistry Letters and Reviews*, 5(3): 303-313.

Umoren, S.A., Eduok, U.M., Solomon, M.M., & Udoh, A.P., (2016) Corrosion inhibition by leaves and stem extracts of Sida acuta for mild steel in 1 M H_2SO_4 solutions investigated by chemical and spectroscopic techniques. *Arabian Journal of Chemistry*, 9: 209-224.

Uwah, I.E., Okafor, P.C., & Ebiekpe, V.E., (2013) Inhibitive action of ethanol extracts from Nauclea latifolia on the corrosion of mild steel in H_2SO_4 solutions and their adsorption characteristics. *Arabian Journal of Chemistry,* 6: 285-293.

Valentine, A., Onukwuli, O., Omotioma, M., & Okafor, N.A., (2018) Optimization and Electrochemical Study on the Control of Mild Steel Corrosion in Hydrochloric Acid Solution with Bitter Kola Leaf Extract as Inhibitor. *South African Journal of Chemistry*, 71: 51-61.

Vargel, C. (2020). Intergranular corrosion. *Corrosion of Aluminium,* 185–197. doi:10.1016/b978-0-08-099925-8.

Verma, A. & Singh, V., (2016) Human Hair: A Biodegradable Composite Fiber–A Review. *International Journal of Waste Resources*, 6(2): 1-4.

Verma, C., Ebenso, C., & Quraishi, M. A., (2017) Chromeno-carbonitriles as corrosion inhibitors for mild steel in acidic solution: electrochemical, surface and computational studies. *Journal of Molecular Liquids,* 233: 403-414

Verma, C., Ebenso, E. E., Bahadur, I., & Quraishi, M. A., (2018) An overview on plant extracts as environmental sustainable and green corrosion inhibitors for metals and alloys in aggressive corrosive media. *Journal of Molecular Liquids,* 266: 577-590.

Verma, C., Olasunkanmi, L., Obot, I., Ebenso, E. & Quraishi, M., (2016) 2,4-Diamino-5-(phenylthio)-5H-chromeno [2,3-b] pyridine-3-carbonitriles as green and effective corrosion inhibitors: gravimetric, electrochemical, surface morphology and theoretical studies. *RSC- Adavances,* 6: 53933-53948.

Verma, C., Quraishi, M. A., Ebenso, E., & Bahadur, I., (2018) A Green and Sustainable Approach for Mild Steel Acidic Corrosion Inhibition Using Leaves Extract: Experimental and DFT Studies. *Journal of Bio- and Tribo-Corrosion*, 4: 33. DOI: 10.1007/s40735-018-0150-3.

Wang, Q., Tan, B., Bao, H., Xie, Y., Mou, Y., Li, P., & Yang, W., (2019) Evaluation of Ficus tikoua leaves extract as an eco-friendly corrosion inhibitor for carbon steel in HCl media. *Bioelectrochemistry,* 128: 49–55.

Xiao, Y., Azaiez, J., & Hill, J. M., (2018) Erroneous Application of Pseudo-Second-Order Adsorption Kinetics Model: Ignored Assumptions and Spurious Correlations. *Industrial & Engineering Chemistry Research*, 57(7): 2705-2709.

Xie, X., & Holze, R., (2018). Experimental methods in corrosion research. *ChemTexts,* 4(1): 1-13.

Xu, P., Zhou, J., Li, G., Wang, P., Wang, P., Li, F., Zhang, B., & Chi, H., (2021) Corrosion inhibition efficiency of compound nitrite with D-sodium gluconate on carbon steel in simulated concrete pore solution. *Construction and Building Materials,* 288: 123101. DOI: 10.1016/j.conbuildmat.2021.123101.

Yaro, A., Khadom, A., & Wael, R., (2013). Apricot juice as green corrosion inhibitor of mild steel in phosphoric acid. *Alexandria Engineering Journal*, *52*(1): 129-135.

Zarrok, H., Zarrouk, A., Salghi, R., Hammouti, B., Elbakri, M., Touhami, M., Bentiss, F., & Oudda, H., (2014) Study of a cysteine derivative as a corrosion inhibitor for carbon steel in phosphoric acid solution. *Research on Chemical Intermediates*, 40: 801–815.

Zhang, W., Wu, Y., & Li, H., (2021) *Apostichopus japonicus polysaccharide* as efficient sustainable inhibitor for mild steel against hydrochloric acid corrosion. *Journal of Molecular Liquids*, 321: 114923. DOI: 10.1016/j.molliq.2020.114923.

Zheng, X., Gong, M., Li, Q., & Guo, L., (2018) Corrosion inhibition of mild steel in sulfuric acid solution by loquat (Eriobotrya japonica Lindl.) leaves extract. *Scientific Reports*, 8(1), 1-15.

Znini, M., Costa, J., & Majidi, L., (2012) Essential oil of *Salvia aucheri mesatlantica* as green inhibitor for the corrosion of steel in 0.5 M H_2SO_4. *Arabian Journal of Chemistry*, 5(4): 467-474.

APPENDICES

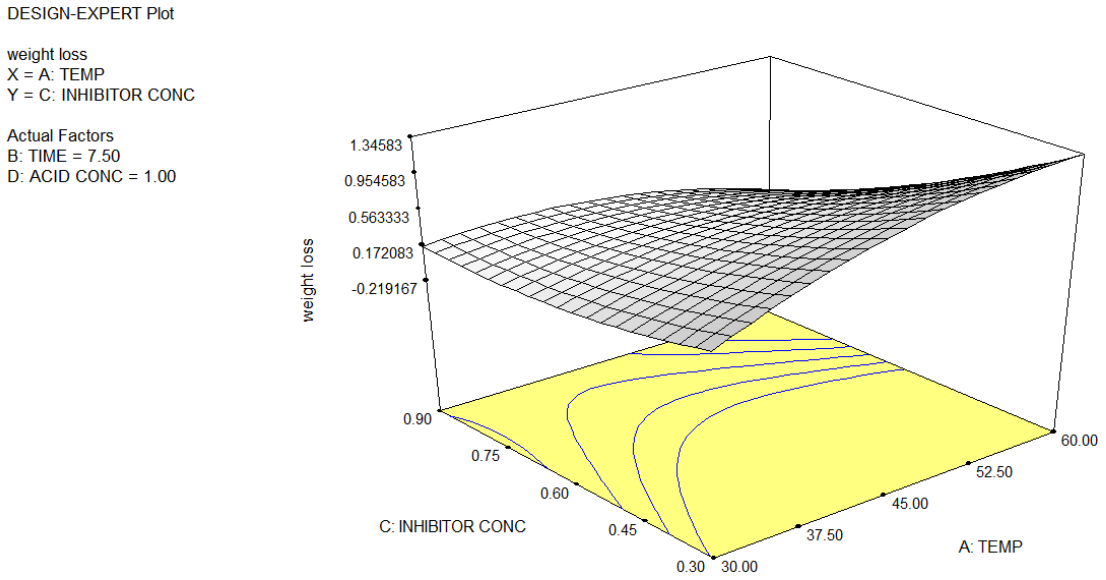

APPENDIX I: 3-D model plot for weight loss of inhibitor concentration versus temperature

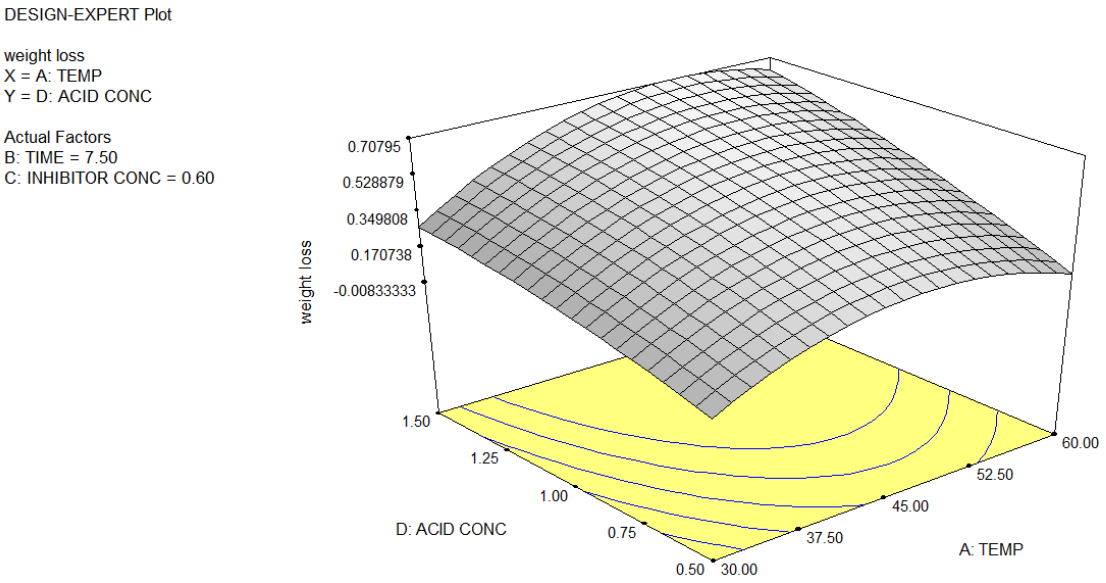

APPENDIX II: 3-D model plot for weight loss of acid concentration versus temperature

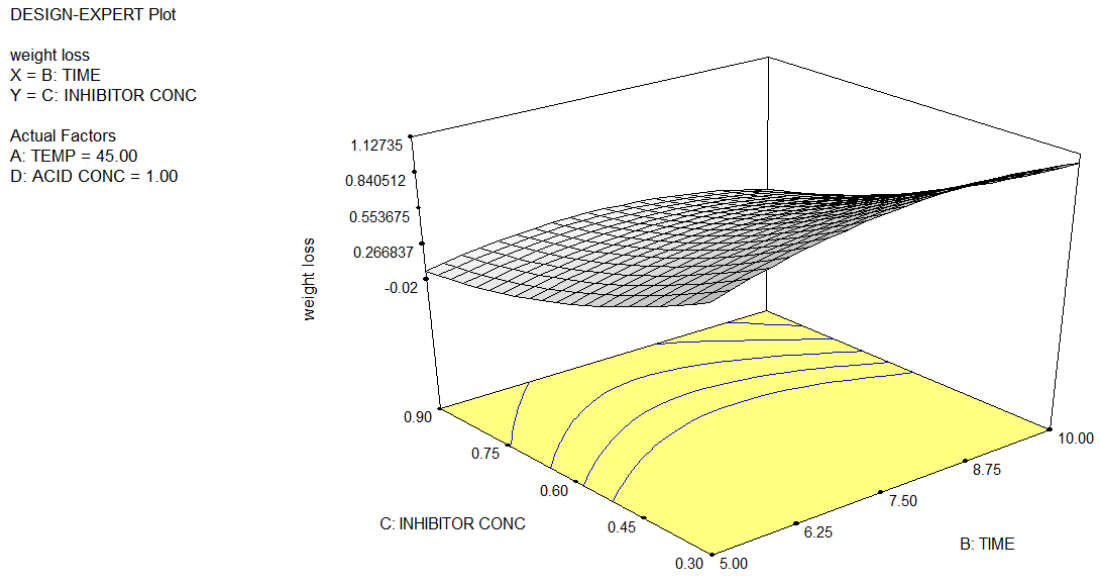

APPENDIX III: 3-D model plot for weight loss of inhibitor concentration versus time

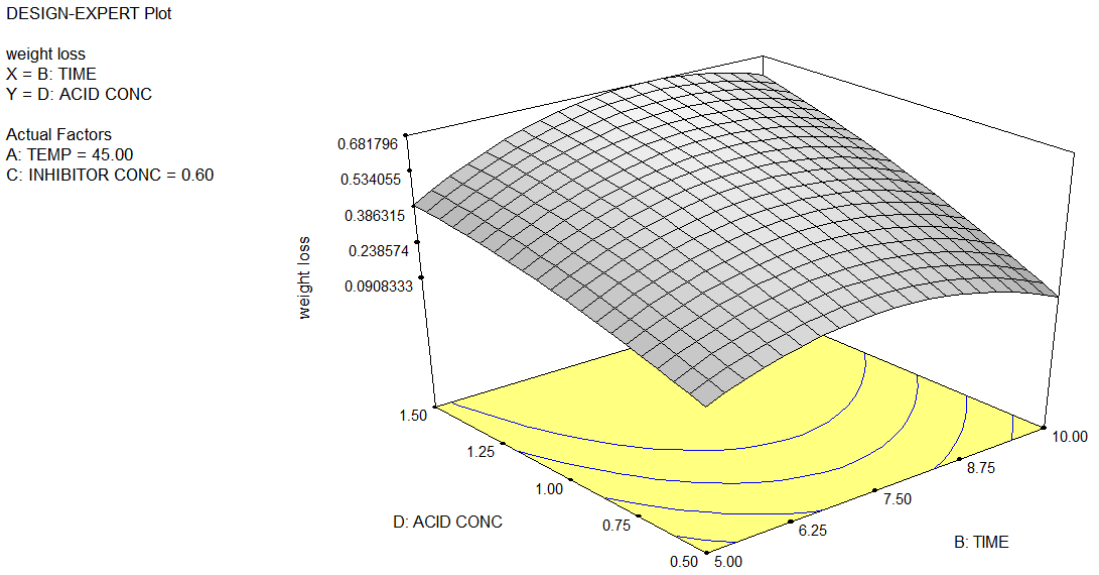

APPENDIX IV: 3-D model plot for weight loss of acid concentration versus time

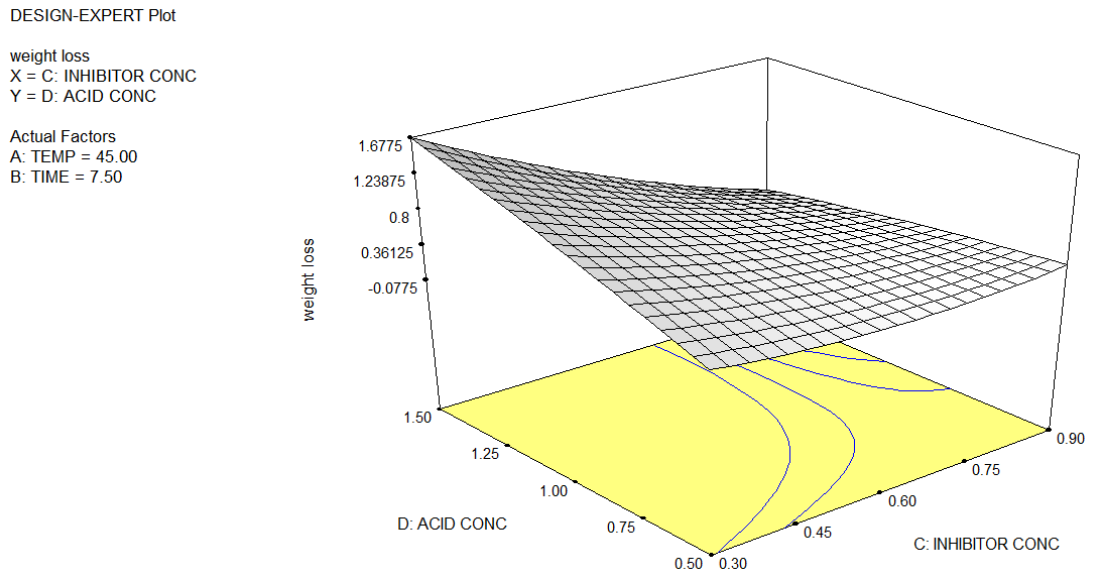

APPENDIX V: 3-D model plot for weight loss of acid concentration versus inhibitor concentration

APPENDIX VI: Quantitative values for bioactive compounds in IBLE

Test	**Quantity (mg/100g)**
Saponins	0.832
Steroid	0.321
Phenol	1.341
Tannin	0.439
Glycoside	0.241
Flavonoid	--
Alkaloid	--

APPENDIX VII: Calculation for the Preparation of H_3PO_4

$$Molarity = \frac{mass\ concentration}{molar\ mass}$$

Molecular weight of H_3PO_4 = 98

Density = 1700 g/dm^3

Percentage purity of acid = 85%

Every 100 g of H_3PO_4 acid contains 85% of solute

Thus, the molarity from which the concentrations of the acid were prepared was 14.745 mol/dm^3.

Concentration of the acid was calculated using Equation 3.2.

$$C_1V_1 = C_2V_2$$

Where: C_1 = 0.5 M, V_2 = 33.9 ml; C_1 = 1.0 M, V_2= 67.8 ml; C_1 = 1.5 M, V_2 = 101.7 ml

As a result, 33.9 ml, 67.8 ml, and 101.7 ml of phosphoric acid solution were made up to 1000 cm^3 in a 1 litre standard flask for 0.5 M, 1.0 M, and 1.5 M concentrations, respectively.